

Smoothing interpolation of five-axis tool path with less feedrate fluctuation and higher computation efficiency

Shujie Sun ^{a,*}, Peng Zhao ^a, Tao Zhang ^a, Beibei Li ^{b,c}, Dong Yu ^{b,c}

^a School of Electromechanical and Automotive Engineering, Yantai University, Yantai 264005, China

^b National Engineering Research Center for High-End CNC, Shenyang Institute of Computing Technology, University of Chinese Academy of Sciences, Liaoning 110168, Shenyang, China

^c Shenyang CASNC Technology Co., Ltd., Shenyang 110168, China

ARTICLE INFO

Keywords:

Five-axis
Feedrate fluctuation
Computation efficiency

ABSTRACT

Five-axis machine tools are widely used in aerospace, die and mold industries. Most of the time, the tool path is described by connecting a series of short linear segments. The tangency discontinuity of the linear segments leads to the discontinuity of the kinematic profiles, hence generating discontinuous interpolation points, and resulting in fluctuation of machine motion, which reduces the machining efficiency and causes excessive tracking and contouring errors. This paper aims to generate smooth interpolation points at servo sample intervals with the proposed G^2 continuous five-axis corner rounding algorithm suitable for reducing feedrate fluctuation along the smoothed toolpath and improving machining efficiency, and the modified jerk-limited feedrate planning algorithm suitable for eliminating feedrate fluctuation within the feedrate planning units and improving interpolation computation efficiency. In this paper, the five-axis linear segments are first smoothed by curvature-optimized cubic Bezier splines, which reduces the number of the feedrate planning units along the smoothed toolpath and improves machining efficiency. Then, the jerk-limited feedrate planning algorithm is modified to ensure that the time interval of each different scheduled feedrate phase is an integer multiple of the axis position control loop closure time (i.e. servo sample interval), which eliminates the feedrate fluctuation within each feedrate planning unit and reduces the interpolation computation load of position command in each interpolation period (i.e. servo sample interval). At last, the effectiveness of the proposed algorithm is demonstrated with simulations and experiments following a five-axis, curved tool path on a CNC (Computer Numerical Control) machine tool.

1. Introduction

Five-axis machine tools are widely used as a highly productive method in industries to produce freeform parts. High-speed and high-quality five-axis CNC machining requires a smooth motion of five-axis machine tools, which involves smooth interpolation of smooth toolpath at fixed control intervals. To generate smooth interpolation points, the five-axis tool path must be geometrically continuous and followed with a smooth feedrate profile. However, the five-axis tool path is described industrially in the G01 code. This description consists of a series of small linear segments and generates tangential discontinuities at each connection point between the linear path segments, i.e. corners. To avoid a full stop at each corner while respecting the jerk limits of machine tool axes, the CNC has to modify the geometry of the tool path

within a set tolerance.

In the literature, the global smoothing method and local smoothing method are available to deal with the smoothness of the tool path, which are respectively suitable for smoothing a portion of the tool path composed of a high density of linear segments and the tool path composed of long linear segments. The global smoothing method converts linear segments into spline curves within a given contour tolerance around the programmed segments. This method has been studied in three-axis machining based on different splines such as quintic splines [1], Bezier splines [2], B-splines [3,4] and NURBS splines [5], while the orientation in five-axis machining has also been smoothed by quaternions [6,7], spherical B-splines [8–10] and position and orientation curves [11–13], etc. Although dominant points are introduced to improve smoothing efficiency, and different geometric deviation models

* Corresponding author.

E-mail address: sunshujie@ustc.edu (S. Sun).

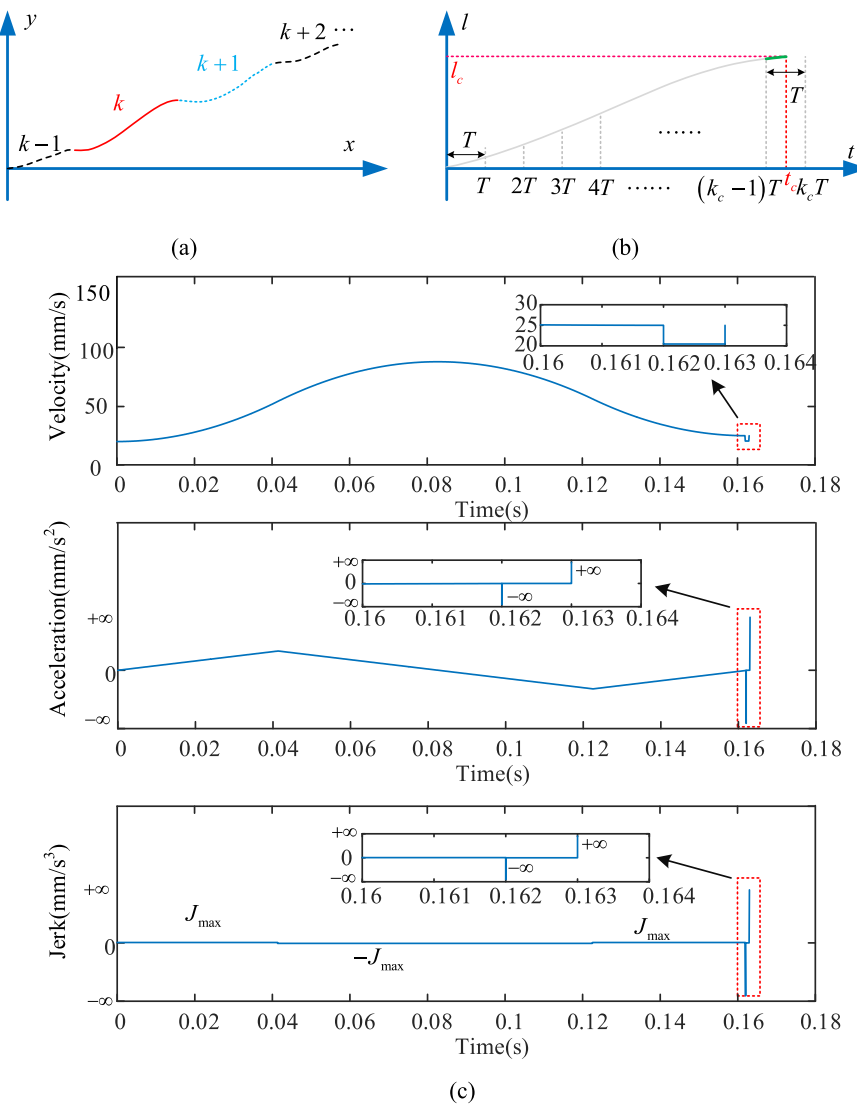


Fig. 1. Illustration of the feedrate fluctuation within the feedrate planning units: (a) four consecutive feedrate planning units; (b) scheduled tool travel displacement for the k th feedrate planning unit; (c) discontinuous kinematic profiles within the last interpolation period of the k th feedrate planning unit.

are constructed to control smoothing errors [4], global smoothing is still computationally time-consuming and difficult to precisely avoid oscillations and respect pre-defined error tolerance limit [14]. Alternatively, local smoothing has been extensively studies in three-axis machining [15–19] and five-axis machining [20–24] to generate tool path with at least G^2/C^2 continuity in the workpiece coordinate system (WCS) [20,22,24] or machine coordinate system (MCS) [21,23] based on different splines such as Bezier splines [15,21,24], B-splines [16–18,20,22,23] and NURBS splines [19]. Due to the advantages in smoothing efficiency and machining quality, local smoothing techniques have also received increasing research attraction and widely implemented in obstacle-avoidance path planning for intelligent vehicles and unmanned aerial vehicles [25,26] and in linear toolpath smoothing for robotic machining [27–29] in recent years. As an example, the quintic B-spline based local transition model proposed by Tulsyan and Altintas [22] is not only applied to five-axis machine tools machining [22,23], but also utilized to obtain smooth tool paths for a 6-DoF (degree of freedom) robot with serial kinematics [27], a 5-DoF machining robot with parallel kinematics [28] and a 5-DOF hybrid machining robot [29]. These local smoothing methods [15–24,27–29] insert a satisfying corner transition curve to the corner in terms of contour error and continuity management. After the tool path is smoothed [1–24,27–29], it is divided

into different feedrate planning units as per the curvature. In high-speed and high-precision machining, short feedrate planning units bring in the fluctuation of the feedrate, and the frequent fluctuations in acceleration and deceleration lead to varying cutting load, resulting in low machining efficiency, poor surface texture and roughness [30,31]. To reduce fluctuation due to unnecessary acceleration/deceleration and optimize the feedrate profile, the feedrate and acceleration look-ahead algorithms are respectively introduced in Refs. [32, 33] and Ref. [34], while a feedrate planning units merging algorithm is proposed by Dong et al. [31]. Since nominal maximum velocity in feedrate planning is constrained by the curvature extremum of transition splines, the reduction of maximum spline curvature [18,19,35,36] is adopted to reduce the magnitude of the feedrate fluctuation. Huang et al. [18] presented a method to reduce the maximum curvature of the local transition B-spline by adjusting the positions of control points. Du and Wang [19] proposed an analytical weight model to reduce the extreme curvature of the NURBS transition spline and avoid additional maximal curvatures on the given transition curve as much as possible. Yan et al. [35] constructed asymmetrical transition curves with quintic B-spline on three-axis toolpath to reduce the curvature extremes and further extended this method to five-axis short-segmented toolpath [36]. But none of the above-mentioned global smoothing methods or local

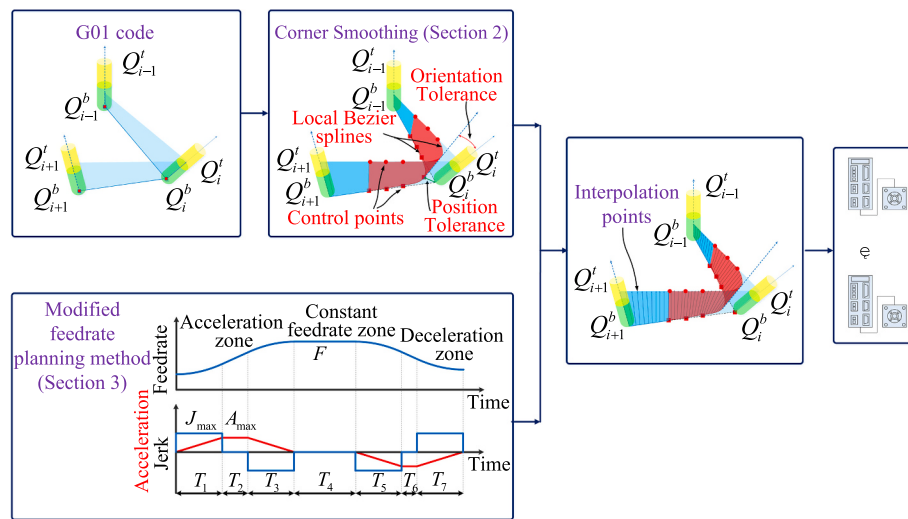


Fig. 2. Smoothing interpolation of five-axis tool path.

smoothing methods reduce the number of feedrate planning units by analytically optimizing spline curvature, thereby reducing feedrate fluctuations along the smoothed toolpath.

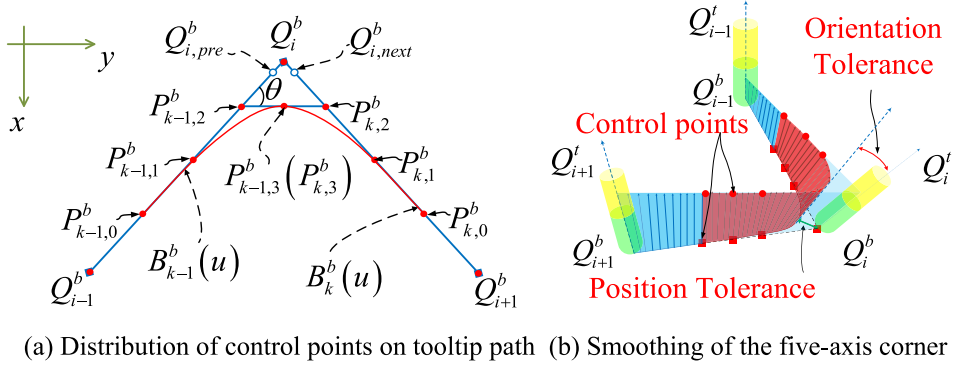
Once the division of the feedrate planning units is carried out, the feedrate planning method has to be performed to generate smooth interpolation points. The jerk [37–39] or jounce [40,41] are limited in interpolation points planning to produce a smooth feedrate profile, but the nonlinear relationship between the arc displacement and the spline parameter induces inaccurate calculation of the interpolation points, i.e. feedrate fluctuation within the interpolation periods. To achieve higher accuracy calculation of the interpolation parameters, Yeh and Hsu applied Taylor's expansion to calculate the spline parameters [42]. Jia et al. [43] and Zhang et al. [44] used Runge–Kutta method and co-lateral triangle deviation (CTD)-based parameter compensation interpolation method to compensate the calculated parameter, respectively. Erkorkmaz and Altintas [1] proposed a quintic spline interpolation technique where the spline parameter is readjusted at every interpolation step for constant path increment interpolation. Heng and Erkorkmaz [45] presented a feed correction polynomial method to evaluate the accurate parameter of interpolation points for constant interpolation period interpolation. These literature [1,42–45] improved the calculation accuracy of spline parameters to yield desired arc displacement and reduce feedrate fluctuation, while Zhao et al. [46] asserted the discrepancy between the target trajectory and the desired tool path is also an important reason that causes feedrate fluctuations within interpolation periods, and presented a feedback interpolator to eliminate the feedrate fluctuation. However, as illustrated in Fig. 1, the machining cycle time of each feedrate planning unit is also desired to be an integer multiple of the axis position control loop closure time, which is important to eliminate the feedrate fluctuation within each feedrate planning unit and improve the computation efficiency of position commands. In Fig. 1(a), a smooth toolpath is divided into four consecutive feedrate planning units (Fig. 1a), and the arc length of the k th unit is l_c . In Fig. 1(b), T denotes the axis position control loop closure time, i.e. the interpolation period of the CNC system, and the machining cycle time of the k th unit scheduled by the jerk-limited feedrate planning algorithm [31] is t_c . Most commonly, t_c is not an integer multiple of T . Just in case the actual machining feedrate exceeds the scheduled feedrate at the end of the k th unit and hence deteriorates the geometrical accuracy of the part, the arc length highlighted by the green line (Fig. 1b) should be travelled in the time interval of $((k_c - 1)T, k_c T]$ rather than $((k_c - 2)T, (k_c - 1)T]$. However, this strategy leads to feedrate fluctuation and abrupt changes in acceleration and jerk (Fig. 1c), which is defined as feedrate fluctuation within the feedrate planning units in this paper and may excite

machine tool's structural modes and hence gives more transient vibrations during high-speed positioning. To solve this problem, Du et al. [47] quantized the number of interpolation periods for different feedrate phases as the nearest integer less than or equal to the number of interpolation periods and eliminated the resulting round-off error of tool travel displacement with an arc length compensation strategy. However, the errors compensated in each interpolation period are not calculated based on the mathematical derivation of kinematic formulations, hence inevitably leading to undesired kinematic characteristics, such as acceleration or jerk that exceed limits.

The goal of this paper is to propose an interpolation points generation method to achieve smooth motion of machine tools as outlined in Fig. 2. Point Q_{i-1}^t and point Q_{i-1}^b define the tool axis orientation on the tool tip path and on the tool axis, respectively. $Q_{i-1}^b Q_i^b Q_{i+1}^b$ and $Q_{i-1}^t Q_i^t Q_{i+1}^t$ are the corners on the lower and upper sides of the tool path and are respectively rounded with Bezier splines to keep G^2 continuity at the junctions (Q_i^b, Q_i^t). For every inserted Bezier transition spline, the control points are adjusted to keep the synchronization of the tool orientation and the tip position, and ensure monotonic curvature for reducing the number of feedrate planning units along the smoothed toolpath. Then, the smoothed tool path is interpolated by jerk-limited feedrate planning algorithm to generate smooth interpolation points. To eliminate the feedrate fluctuation within the feedrate planning units, the time interval of each feedrate phase of an arbitrary feedrate planning unit is adjusted to have an integer multiple of the interpolation period, on this basis, the computation time of each interpolation point is further optimized. Some of the key contributions of this paper are:

- (1) Feedrate fluctuation along the smoothed toolpath is reduced and the machining efficiency is improved by the curvature-optimized tool path smoothing algorithm.
- (2) Feedrate fluctuation within the feedrate planning units is eliminated with the modified feedrate planning algorithm.
- (3) With an integer multiple of the interpolation period in each feedrate phase of an arbitrary feedrate planning unit, the modified feedrate planning algorithm also improves the computation efficiency of interpolation points.
- (4) The simulation and experimental results demonstrate that the proposed algorithm improves the machining efficiency, has higher tracking accuracy and smaller contour error.

The paper is organized as follows. The five-axis toolpath corner smoothing algorithm with G^2 continuity and monotonic curvature is



(a) Distribution of control points on tooltip path (b) Smoothing of the five-axis corner

Fig. 3. Corner smoothing algorithm for five-axis tool path. (a) Distribution of control points on tooltip path. (b) Smoothing of the five-axis corner.

presented in [Section 2](#), followed by the modified jerk-limited feedrate planning algorithm and optimized interpolation point calculation method in [Section 3](#). The proposed algorithm is proven with simulation and experimental results in [Section 4](#) followed by concluding remarks in [Section 5](#).

2. Five-axis corner smoothing algorithm

2.1. Corner smoothing of tooltip position

Bezier splines are constructed for each corner. Let $C(u)$ represents a n th-degree Bezier spline curve as follows [48]:

$$C(u) = \sum_{i=0}^n b_{i,n}(u)P_i \quad 0 \leq u \leq 1 \quad (1)$$

where P_i are control points, and $b_{i,n}(u)$ are basis functions defined as:

$$b_{i,n}(u) = \frac{n!}{i!(n-i)!} u^i (1-u)^{n-i} \quad (2)$$

The first and second derivatives of $C(u)$ are given as follows:

$$\left. \begin{aligned} C'(u) &= n \sum_{i=0}^{n-1} b_{i,n-1}(u)(P_{i+1} - P_i) \\ C''(u) &= n(n-1) \sum_{i=0}^{n-2} b_{i,n-2}(u)(P_{i+2} - 2P_{i+1} + P_i) \end{aligned} \right\} \quad (3)$$

As illustrated in [Fig. 3\(a\)](#), $Q_{i-1}^b, Q_i^b, Q_{i+1}^b$ are tooltip points retrieved from NC code, transition curves inserted into the corner ($Q_{i-1}^b, Q_i^b, Q_{i+1}^b$) are constructed with two cubic Bezier splines (B_{k-1}^b, B_k^b) connected at point $P_{k-1,3}^b \equiv P_{k,3}^b$, which have the following form:

$$\left. \begin{aligned} B_{k-1}^b(u) &= P_{k-1,0}^b b_{0,3}(u) + P_{k-1,1}^b b_{1,3}(u) + P_{k-1,2}^b b_{2,3}(u) + P_{k-1,3}^b b_{3,3}(u) \\ B_k^b(u) &= P_{k,3}^b b_{0,3}(u) + P_{k,2}^b b_{1,3}(u) + P_{k,1}^b b_{2,3}(u) + P_{k,0}^b b_{3,3}(u) \end{aligned} \right\} \quad (4)$$

where $k = 2(r-1)$ and r is the sequence number of the tooltip points; $P_{k-1,j}^b$ and $P_{k,j}^b$ ($j = 0, \dots, 3$) are the controls points of Bezier splines B_{k-1}^b and B_k^b respectively, and are symmetric about the angle bisector $Q_i^b P_{k,3}^b$; $l_{k-1,1}^b, l_{k-1,2}^b$ and $l_{k-1,3}^b$ are the length of line segments $Q_i^b P_{k-1,2}^b$, $P_{k-1,2}^b P_{k-1,1}^b$ and $P_{k-1,1}^b P_{k-1,0}^b$, respectively; $l_{k,1}^b, l_{k,2}^b$ and $l_{k,3}^b$ are the length of line segments $Q_i^b P_{k,2}^b$, $P_{k,2}^b P_{k,1}^b$ and $P_{k,1}^b P_{k,0}^b$, respectively. Because the control points $P_{k,j}^b$ ($j = 0, 1, 2$) are collinear and located on the same line segment $Q_i^b Q_{i+1}^b$, spline $B_k^b(u)$ is tangent to line segment $Q_i^b Q_{i+1}^b$ at junction point $P_{k,0}^b$. Combing with the curvature at point $P_{k,0}^b$ is zero, $B_k^b(u)$ and $Q_i^b Q_{i+1}^b$ have G^2 continuity at point $P_{k,0}^b$. Similarly, $B_{k-1}^b(u)$ has G^2 continuity with $Q_{i-1}^b Q_i^b$ at junction point $P_{k-1,0}^b$. The symmetry between

$P_{k-1,j}^b$ and $P_{k,j}^b$ ($j = 0, \dots, 3$) ensures G^2 continuity of $B_{k-1}^b(u)$ and $B_k^b(u)$ at point $P_{k,3}^b \equiv P_{k-1,3}^b$. Hence, the tooltip path defined by $B_{k-1}^b(u)$ and $B_k^b(u)$ is G^2 continuous.

By letting $l_{k,2}^b = \alpha l_{k,1}^b$ and $l_{k,3}^b = \beta l_{k,1}^b$, the control points of tooltip position transition spline curves ($B_{k-1}^b(u), B_k^b(u)$) can be obtained as follows:

$$\left. \begin{aligned} P_{k-1,0}^b &= Q_i^b + l_{k-1,1}^b (1 + \alpha + \beta) \overrightarrow{Q_i^b Q_{i-1}^b} / \| \overrightarrow{Q_i^b Q_{i-1}^b} \|, \\ P_{k-1,1}^b &= Q_i^b + l_{k-1,1}^b (1 + \alpha) \overrightarrow{Q_i^b Q_{i-1}^b} / \| \overrightarrow{Q_i^b Q_{i-1}^b} \|, \\ P_{k-1,2}^b &= Q_i^b + l_{k-1,1}^b \overrightarrow{Q_i^b Q_{i-1}^b} / \| \overrightarrow{Q_i^b Q_{i-1}^b} \|, \\ P_{k-1,3}^b &= Q_i^b + l_{k-1,1}^b \sin \theta \overrightarrow{Q_i^b P_{k-1,3}^b} \end{aligned} \right\} \quad (5)$$

where $\overrightarrow{Q_i^b P_{k-1,3}^b} = (\overrightarrow{Q_i^b Q_{i-1}^b} / \| \overrightarrow{Q_i^b Q_{i-1}^b} \| + \overrightarrow{Q_i^b Q_{i+1}^b} / \| \overrightarrow{Q_i^b Q_{i+1}^b} \|) / \| \overrightarrow{Q_i^b Q_{i-1}^b} / \| \overrightarrow{Q_i^b Q_{i+1}^b} \| + \overrightarrow{Q_i^b Q_{i+1}^b} / \| \overrightarrow{Q_i^b Q_{i+1}^b} \| \|$, $\theta = \angle Q_i^b P_{k-1,2}^b P_{k-1,3}^b$.

$$\left. \begin{aligned} P_{k,0}^b &= Q_i^b + l_{k,1}^b (1 + \alpha + \beta) \overrightarrow{Q_i^b Q_{i+1}^b} / \| \overrightarrow{Q_i^b Q_{i+1}^b} \|, \\ P_{k,1}^b &= Q_i^b + l_{k,1}^b (1 + \alpha) \overrightarrow{Q_i^b Q_{i+1}^b} / \| \overrightarrow{Q_i^b Q_{i+1}^b} \|, \\ P_{k,2}^b &= Q_i^b + l_{k,1}^b \overrightarrow{Q_i^b Q_{i+1}^b} / \| \overrightarrow{Q_i^b Q_{i+1}^b} \|, \\ P_{k,3}^b &= Q_i^b + l_{k,1}^b \sin \theta \overrightarrow{Q_i^b P_{k,3}^b} \end{aligned} \right\} \quad (6)$$

The relationship between the corner transition error e and $l_{k,1}^b$ is obtained as $e = l_{k,1}^b \sin \theta$. To avoid the intersection of adjacent transition Bezier splines, $l_{k,1}^b$ should not exceed half of $\| \overrightarrow{Q_i^b Q_{i-1}^b} \|$ and $\| \overrightarrow{Q_i^b Q_{i+1}^b} \|$. Since transition error e should be smaller than the approximation error tolerance e_{\max} , $l_{k,1}^b$ is evaluated as:

$$l_{k,1}^b = \min \left(e_{\max} / \sin \theta, \left\| \overrightarrow{Q_i^b Q_{i+1}^b} \right\| / (2(\alpha + \beta + 1)), \left\| \overrightarrow{Q_i^b Q_{i-1}^b} \right\| / (2(\alpha + \beta + 1)) \right) \quad (7)$$

The control points of splines ($B_{k-1}^b(u), B_k^b(u)$) and the length of line segment $Q_i^b P_{k,2}^b$ (i.e. $l_{k,1}^b$) can be evaluated from the values of α and β , which are obtained by imposing toolpath synchronization constraint in the following [Section 2.2](#) “Synchronization of the toolpath”. It should be noted here that the control points of transition spline curves ($B_{k-1}^t(u), B_k^t(u)$) for the tool orientation path can be obtained similarly to that of spline curves ($B_{k-1}^b(u), B_k^b(u)$) and are not discussed in detail here for brevity.

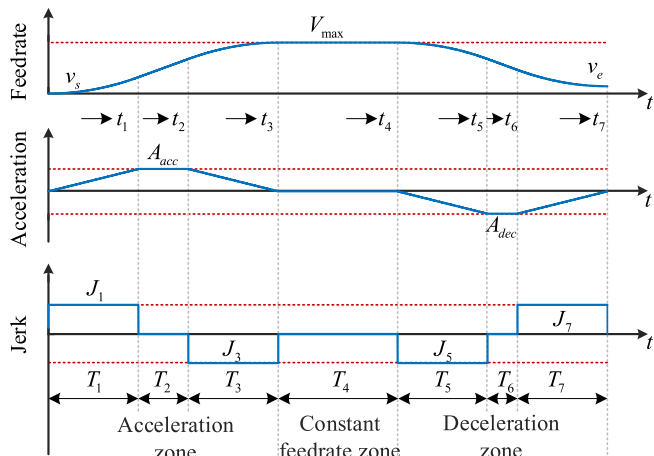


Fig. 4. A complete jerk-limited feedrate profile.

2.2. Synchronization of the toolpath

Five-axis tool path defined by two pairs of Bezier splines, one at the tool-tip ($B_{k-1}^b(u), B_k^b(u)$) and the other is with an offset along the tool axis ($B_{k-1}^t(u), B_k^t(u)$), is smoothed by the G^2 continuity algorithms given in Section 2.1. However, the smooth motion of the tool also depends on the variation in tool orientation with respect to the tooltip displacement ($dOri/ds, d^2Ori/ds^2$), which must be kept continuous at the junction points of tool path segments. Otherwise, abrupt changes in the tool orientation during interpolation will lead to high acceleration/jerk spikes which would damage the surface finish and reduce machining accuracy. Once the bottom and top tool paths are smoothed by Bezier splines in the workpiece coordinate frame, the orientation of the tool can be given by the bottom and top tool paths as:

$$Ori = \frac{B_k^t(u') - B_k^b(u')}{\|B_k^t(u') - B_k^b(u')\|} \quad (8)$$

Therefore, the derivatives of the tool axis orientation are evaluated as:

$$\left. \begin{aligned} \frac{dOri}{ds} &= \frac{B_k^{t'}(u') - B_k^{b'}(u')}{\|B_k^t(u') - B_k^b(u')\|} u_s^b \\ \frac{d^2Ori}{ds^2} &= \frac{1}{\|B_k^t(u') - B_k^b(u')\|} \left[(B_k^{t''}(u') - B_k^{b''}(u')) (u_s^b)^2 + (B_k^{t'}(u') - B_k^{b'}(u')) u_{ss}^b \right] \end{aligned} \right\} \quad (9)$$

where $B_k^{t'} = dB^t(u)/du^t$, $B_k^{b'} = dB^b(u)/du^b$, $u^t = u^b$, $u_s^b = \frac{1}{\|B_k^b(u^b)\|}$, and $u_{ss}^b = -\frac{\langle B_k^b(u^b), B_k^{b''}(u^b) \rangle}{\|B_k^b(u^b)\|^3}$.

If the first and second derivatives of orientation ($dOri/ds, d^2Ori/ds^2$) are matched at junction points ($P_{k,3}^b, P_{k,0}^b$), the motion of tool orientation and tip position on tool path ($B_k^t(u), B_k^b(u)$) are continuous with the previous and next five-axis tool path segments.

To synchronize the tool orientation and the tip position and keep the monotonic curvature for the transition Bezier spline, the parameters (α, β) are evaluated as follows:

- (a) The first and second derivatives of the bottom and top transition Bezier curves ($B_k^t(u), B_k^b(u)$) at the ending points ($u = 1$) can be evaluated as:

$$\left. \begin{aligned} C^{b'}(1) &= 3\beta l_{k,1}^b \overrightarrow{Q_i^b Q_{i+1}^b} / \|\overrightarrow{Q_i^b Q_{i+1}^b}\|, \\ C^{b''}(1) &= 6(\beta - \alpha) l_{k,1}^b \overrightarrow{Q_i^b Q_{i+1}^b} / \|\overrightarrow{Q_i^b Q_{i+1}^b}\|, \\ C^t(1) &= 3\beta l_{k,1}^t \overrightarrow{Q_i^t Q_{i+1}^t} / \|\overrightarrow{Q_i^t Q_{i+1}^t}\|, \\ C^{t''}(1) &= 6(\beta - \alpha) l_{k,1}^t \overrightarrow{Q_i^t Q_{i+1}^t} / \|\overrightarrow{Q_i^t Q_{i+1}^t}\| \end{aligned} \right\} \quad (10)$$

Substituting Eq. (10) into Eq. (9), Eq. (11) is obtained (Appendix A).

$$\left. \begin{aligned} \frac{P_{k,0}^t - P_{k,1}^t}{P_{k,0}^b - P_{k,1}^b} &= \frac{\overrightarrow{Q_{i+1}^t} - \overrightarrow{Q_i^t}}{\overrightarrow{Q_{i+1}^b} - \overrightarrow{Q_i^b}} \\ \alpha &= \beta \end{aligned} \right\} \quad (11)$$

Combining Eq. (5), the curvature on curve $B_k^b(u)$ is evaluated as:

$$\kappa = \frac{\|B_k^{b'}(u) \times B_k^{b''}(u)\|}{\|B_k^{b'}(u)\|^3} = \frac{m}{3l_1 n^{3/2}} \quad (12)$$

where $m = \sin(2\theta)\alpha(1-u)$, $n = \cos^2\theta[(u-1)^2 - \alpha u(u-2)]^2 + \alpha^2 u^2 \sin^2\theta(u-2)^2$.

Then, the first derivative of κ is obtained:

$$\kappa' = \frac{2m' - 3mn'}{6l_1 n^{5/2}} \quad (13)$$

If $\alpha \geq 1$ is satisfied, then $\kappa' < 0$ holds true, i.e. the spline curve $B_k^b(u)$ can be derived to have monotonic curvature (Appendix B).

- (b) To generate a smooth variation of orientation, $dOri/ds$ and d^2Ori/ds^2 should also be continuous at point $P_{k,3}^b \equiv P_{k-1,3}^b$, which yields $\alpha = 1$. (Appendix C)

Hence, the control points of the Bezier spline $B_k^b(u)$ are obtained:

$$\left. \begin{aligned} P_{k,0}^b &= Q_i^b + 3l_{k,1}^b \overrightarrow{Q_i^b Q_{i+1}^b} / \|\overrightarrow{Q_i^b Q_{i+1}^b}\|, \\ P_{k,1}^b &= Q_i^b + 2l_{k,1}^b \overrightarrow{Q_i^b Q_{i+1}^b} / \|\overrightarrow{Q_i^b Q_{i+1}^b}\|, \\ P_{k,2}^b &= Q_i^b + l_{k,1}^b \overrightarrow{Q_i^b Q_{i+1}^b} / \|\overrightarrow{Q_i^b Q_{i+1}^b}\|, \\ P_{k,3}^b &= Q_i^b + l_{k,1}^b \sin\theta \overrightarrow{Q_i^b P_{k,3}^b} \end{aligned} \right\} \quad (14)$$

Similarly, the control points of the Bezier spline $B_k^t(u)$ are evaluated as:

$$\left. \begin{aligned} P_{k,0}^t &= Q_i^t + 3l_{k,1}^t \overrightarrow{Q_i^t Q_{i+1}^t} / \|\overrightarrow{Q_i^t Q_{i+1}^t}\|, \\ P_{k,1}^t &= Q_i^t + 2l_{k,1}^t \overrightarrow{Q_i^t Q_{i+1}^t} / \|\overrightarrow{Q_i^t Q_{i+1}^t}\|, \\ P_{k,2}^t &= Q_i^t + l_{k,1}^t \overrightarrow{Q_i^t Q_{i+1}^t} / \|\overrightarrow{Q_i^t Q_{i+1}^t}\|, \\ P_{k,3}^t &= Q_i^t + l_{k,1}^t \sin\theta \overrightarrow{Q_i^t P_{k,3}^t} \end{aligned} \right\} \quad (15)$$

After determining the spline curves $B_k^b(u)$ and $B_k^t(u)$, the corner ($Q_i^b Q_{i+1}^b Q_{i+2}^b$) and ($Q_i^t Q_{i+1}^t Q_{i+2}^t$) are smoothed iteratively. To generate smooth interpolation points, the G^2 continuous tool path is divided into different feedrate planning units based on the curvature and the modified feedrate planning algorithm in Section 3 has to be performed to preserve C^2 continuity in motion.

3. Modified jerk-limited feedrate planning algorithm

In Fig. 4, v_s and v_e are the start and end feedrates of the jerk-limited feedrate profile, respectively; $T_i (i = 1, \dots, 7)$ denotes the time interval of the i th feedrate phase of the feedrate profile; t_i is the end time of the i th

Table 1
Kinematic equations for jerk-limited feedrate profiles.

t	Jerk	Acceleration	Velocity	Displacement
$0 \leq t < t_1$	J_{\max}	$J_{\max}t$	$v_s + J_{\max}t^2/2$	$v_s t + J_{\max}t^3/6$
$t_1 \leq t < t_2$	0	A_{\max}	$v_1 + A_{\max}t$	$s_1 + v_1 t + A_{\max}t^2/2$
$t_2 \leq t < t_3$	—	$A_{\max} - J_{\max}t$	$v_2 + A_{\max}t - J_{\max}t^2/2$	$s_2 + v_2 t + A_{\max}t^2/2 - J_{\max}t^3/6$
$t_3 \leq t < t_4$	J_{\max}	0	v_3	$s_3 + v_3 t$
$t_4 \leq t < t_5$	—	$-J_{\max}t$	$v_4 - J_{\max}t^2/2$	$s_4 + v_4 t - J_{\max}t^3/6$
$t_5 \leq t < t_6$	J_{\max}	0	$v_5 - A_{\max}t$	$s_5 + v_5 t - A_{\max}t^2/2$
$t_6 \leq t \leq t_7$	J_{\max}	$-A_{\max} + J_{\max}t$	$v_6 - A_{\max}t + J_{\max}t^2/2$	$s_6 + v_6 t - A_{\max}t^2/2 + J_{\max}t^3/6$

v_i and $s_i (i = 1, \dots, 6)$ are the feedrate and displacement at time t_i , respectively.

feedrate phase, i.e. $t_i = \sum_{j=1}^{j \leq i} T_j$. As illustrated in Fig. 4, a complete jerk-limited feedrate profile contains an acceleration zone (T_1, T_2, T_3), a constant feedrate zone (T_4) and a deceleration zone (T_5, T_6, T_7); V_{\max} is the maximum value of the scheduled feedrate profile; A_{acc} and A_{dec} are the maximum acceleration and deceleration in the acceleration zone and deceleration zone, respectively; $J_k (k = 1, 3, 5, 7)$ is the maximum jerk in

the k th feedrate phase of the feedrate profile. Assuming that F_c , A_{\max} and J_{\max} are the feedrate, acceleration and jerk limits in the feedrate planning respectively, then $A_{acc} = -A_{dec} = A_{\max}$ and $J_1 = -J_3 = -J_5 = J_7 = J_{\max}$ are established, and the detailed kinematic equations for the jerk-limited feedrate profile can be obtained and summarized in Table 1.

Since $A_{\max} = J_{\max}T_1$ and $T_1 = T_3$ (Fig. 4), the maximum velocity V_{\max} can be reorganized as:

$$V_{\max} = v_s + A_{\max}(T_1 + T_2) \quad (16)$$

Combining,

$$S = \frac{1}{2}A_{\max}(2T_1^2 + 3T_1T_2 + T_2^2) + v_s(2T_1 + T_2) \quad (17)$$

where S is the tool travel displacement at time t_7 .

The travel displacement of the tool in the acceleration zone can be reorganized as:

$$S_{acc} = \frac{v_s + V_{\max}}{2}(2T_1 + T_2) \quad (18)$$

Similarly, travel displacement of the tool in the deceleration zone can be evaluated as:

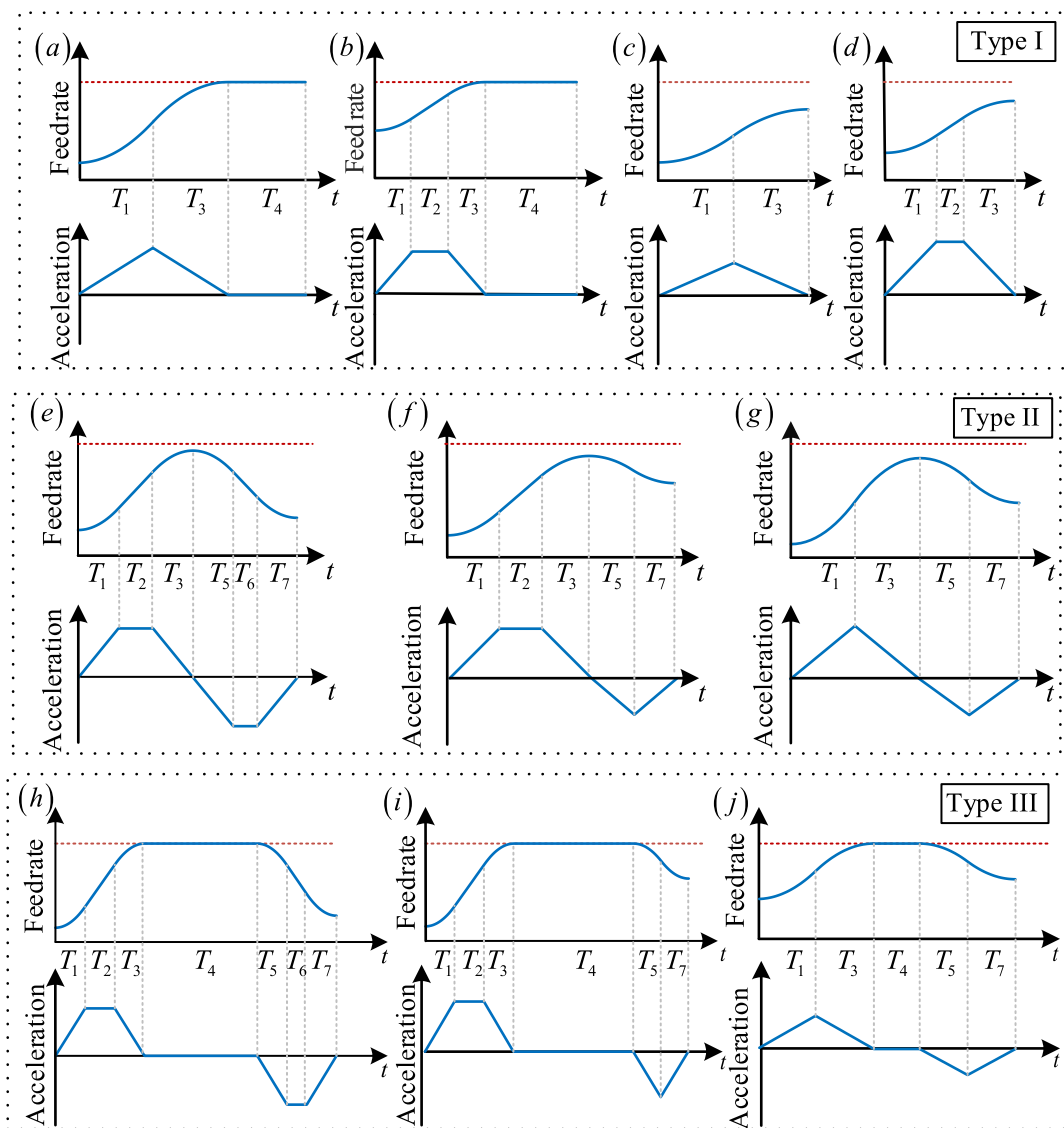


Fig. 5. Different feedrate profiles for $v_s < v_e$: (a–d) Type I; (e–g) Type II; (h–j) Type III.

Table 2Non-zero feedrate phases for different feedrate profile types ($v_s < v_e$).

Type I	$\text{if } v_e - v_s > A_{\max}^2 / J_{\max}, T_1 = T_3 = A_{\max} / J_{\max}, T_2 = (v_e - v_s) / A_{\max} - T_1,$ $\text{else } T_1 = T_3 = \sqrt{(v_e - v_s) / J_{\max}}.$ $\text{if } S_{acc} = S_{segment}, T_4 = 0, \text{else } T_4 = (S_{segment} - S_{acc}) / v_e.$
Type II	$\text{if } V_{\max} - v_s > A_{\max}^2 / J_{\max}, T_1 = T_3 = A_{\max} / J_{\max}, T_2 = (V_{\max} - v_s) /$ $A_{\max} - T_1, \text{else } T_1 = T_3 = \sqrt{(V_{\max} - v_s) / J_{\max}}.$ $\text{if } V_{\max} - v_e > A_{\max}^2 / J_{\max}, T_5 = T_7 = A_{\max} / J_{\max}, T_6 = (V_{\max} - v_e) /$ $A_{\max} - T_5, \text{else } T_5 = T_7 = \sqrt{(V_{\max} - v_e) / J_{\max}}.$
Type III	$\text{if } V_{\max} - v_s > A_{\max}^2 / J_{\max}, T_1 = T_3 = A_{\max} / J_{\max}, T_2 = (V_{\max} - v_s) / A_{\max} - T_1,$ $\text{else } T_1 = T_3 = \sqrt{(V_{\max} - v_s) / J_{\max}}.$ $\text{if } V_{\max} - v_e > A_{\max}^2 / J_{\max}, T_5 = T_7 = A_{\max} / J_{\max}, T_6 = (V_{\max} - v_e) / A_{\max} - T_5,$ $\text{else } T_5 = T_7 = \sqrt{(V_{\max} - v_e) / J_{\max}}.$ $T_4 = (S_{segment} - S_{acc} - S_{dec}) / V_{\max}.$

* V_{\max} is obtained by the method proposed by Dong et al. [31] and $S_{segment}$ is the toolpath lengths of the current feedrate planning unit.

$$S_{dec} = \frac{v_e + V_{\max}}{2} (T_5 + T_6) \quad (19)$$

Hence, the tool travel displacement in the acceleration and deceleration zones ($T_1 + T_2 + T_3 + T_5 + T_6 + T_7$) is evaluated as:

$$S_{no_cons} = aV_{\max} + b \quad (20)$$

where $a = (T_1 + T_5 + T_2/2 + T_6/2)$, $b = v_s(T_1 + T_2/2) + v_e(T_5 + T_6/2)$.

The jerk-limited feedrate planning algorithm is iteratively implemented for each feedrate planning unit along the toolpath, and then the feedrate phases $T_i (i = 1, \dots, 7)$ of every feedrate planning unit can be obtained. To eliminate the feedrate fluctuation within the feedrate planning units and improve the computation efficiency of interpolation points, each feedrate phase is adjusted to have an integer multiple of the interpolation period in this paper. Since the start feedrate (v_s) may be lower than, equal to or higher than the end feedrate (v_e), the adjustment process is discussed separately.

3.1. The start feedrate lower than the end feedrate (i.e. $v_s < v_e$)

Due to the different toolpath lengths of different feedrate planning units, the time intervals of some feedrate phases $T_i (i = 1, \dots, 7)$ of some feedrate planning units may be zero, resulting in different types of feedrate profiles. As illustrated in Fig. 5(a–d), (e–g) and (h–j) are the feedrate profiles without the deceleration zone (feedrate type I), feedrate profiles with an acceleration zone and a deceleration zone (feedrate type II) and feedrate profiles that contain an acceleration zone, a constant feedrate zone and a deceleration zone (feedrate type III) respectively. The non-zero feedrate phases of different feedrate profile types are summarized in Table 2, and the detailed adjustment process of feedrate phases for different feedrate profiles is classified as follows.

(a) Adjustment of feedrate phases for Type I (Fig. 5a–d).

In Fig. 5(a–d), the initial scheduled feedrate profiles only have acceleration and constant feedrate zones, i.e. $T_i = 0 (i = 5, \dots, 7)$. Therefore, only $T_i (i = 1, 2, 3, 4)$ needs to be adjusted to have integer multiples of the interpolation period, where $T_i (i = 1, 2, 3)$ is first revised as:

$$T'_i = \text{ceil}(T_i / T)T \quad (21)$$

Combing Eq. (18), the corresponding tool travel displacement in the revised feedrate phases $T'_i (i = 1, 2, 3)$ is calculated as:

$$S'_{acc} = \frac{v_s + V_{\max}}{2} (2T'_1 + T'_2) \quad (22)$$

which should be no longer than the toolpath length of the current feedrate planning unit ($S_{segment}$) and determines the value of the revised feedrate phase T_4 . Hence,

Case $S'_{acc} < S_{segment}$ holds (Fig. 5a–b): The adjusted feedrate profile must have a constant feedrate zone, and the revised T_4 (T'_4) is evaluated as:

$$T'_4 = \text{ceil}\left(\frac{S_{segment} - S'_{acc}}{V_{\max}T}\right)T = \text{ceil}\left(\frac{S_{segment} - b'}{V_{\max}T} - \frac{a'}{T}\right)T \quad (23)$$

where $a' = (T'_1 + T'_2/2)$, $b' = v_s(T'_1 + T'_2/2)$.

Since the toolpath length of each feedrate planning unit ($S_{segment}$) is constant and only determined by the smoothed toolpath, the maximum velocity (V_{\max}) on the current feedrate planning unit needs further adjustment for the revised $T'_i (i = 1, 2, 3, 4)$ to ensure tool travel displacement shorter than or equal to $S_{segment}$. Considering,

$$\left. \begin{aligned} S'_{acc} &= \frac{v_s + V'_{\max}}{2} (2T'_1 + T'_2) \\ S_{segment} &= S'_{acc} + V'_{\max} T'_4 \end{aligned} \right\} \quad (24)$$

The V_{\max} is revised as:

$$V'_{\max} = \frac{S_{segment} - S'_{acc}}{T'_4} = \frac{S_{segment} - v_s(T'_1 + T'_2/2)}{T'_4 + T'_1 + T'_2/2} \quad (25)$$

Since the revised feedrate phase $T'_i (i = 1, 2, 3, 4)$ and maximum velocity V'_{\max} are now different than the initial scheduled feedrate phase $T_i (i = 1, 2, 3, 4)$ and V_{\max} , while the toolpath length of the current feedrate planning unit is unchanged, it is necessary to modify the end feedrate (v_e), acceleration limit (A_{acc}) and jerk limits (J_1, J_3). Combing with Table 1, the modified end feedrate (v'_e), acceleration limit (A'_{acc}) and jerk limits (J'_1, J'_3) are evaluated as:

$$\left. \begin{aligned} v'_e &= V'_{\max} = \frac{S_{segment} - v_s(T'_1 + T'_2/2)}{T'_4 + T'_1 + T'_2/2} \\ A'_{acc} &= \frac{v'_e - v_s}{T'_1 + T'_2} \\ J'_1 &= -J'_3 = \frac{A'_{acc}}{T'_1} \end{aligned} \right\} \quad (26)$$

Case $S'_{acc} \geq S_{segment}$ holds (Fig. 5a–d): The adjusted feedrate profile does not have the constant feedrate zone, and the initial scheduled T_4 is revised as $T'_4 = 0$. To ensure the S'_{acc} (Eq. (22)) no longer than $S_{segment}$, the maximum velocity (V_{\max}) on the current feedrate planning unit needs further adjustment for the revised $T'_i (i = 1, 2, 3)$. Considering Eq. (20), the V_{\max} is revised as:

$$V'_{\max} = \frac{S_{segment} - b'}{a'} \quad (27)$$

where $a' = (T'_1 + T'_2/2)$, $b' = v_s(T'_1 + T'_2/2)$.

Combing Table 1, the modified acceleration limit (A'_{acc}) and jerk limits (J'_1, J'_3) for revised feedrate phases $T'_i (i = 1, 2, 3)$ are evaluated as:

$$\left. \begin{aligned} v'_e &= V'_{\max} = \frac{S_{segment} - b'}{a'} \\ A'_{acc} &= \frac{V'_{\max} - v_s}{T'_1 + T'_2}, \quad J'_1 = -J'_3 = \frac{A'_{acc}}{T'_1} \end{aligned} \right\} \quad (28)$$

where $a' = (T'_1 + T'_2/2)$, $b' = v_s(T'_1 + T'_2/2)$.

Hence, the revised feedrate phases and kinematic parameters are summarized as:

$$\left\{ \begin{array}{l} T'_i = \text{ceil}(T_i/T)T \quad (i=1,2,3), T'_4 = \text{ceil}\left(\frac{S_{\text{segment}} - b'}{V_{\max}T} - \frac{a'}{T}\right)T, \\ \text{when } S'_{\text{acc}} < S_{\text{segment}} \quad \left\{ \begin{array}{l} T'_5 = T'_6 = T'_7 = 0, \\ v'_e = V'_{\max} = \frac{S_{\text{segment}} - v_s(T'_1 + T'_2/2)}{T'_4 + T'_1 + T'_2/2}, A'_{\text{acc}} = \frac{v'_e - v_s}{T'_1 + T'_2}, J'_1 = -J'_3 = \frac{A'_{\text{acc}}}{T'_1} \end{array} \right. \\ \left. \begin{array}{l} T'_i = \text{ceil}(T_i/T)T \quad (i=1,2,3), T'_4 = T'_5 = T'_6 = T'_7 = 0 \\ v'_e = V'_{\max} = \frac{S_{\text{segment}} - b'}{a'}, \\ A'_{\text{acc}} = \frac{V'_{\max} - v_s}{T'_1 + T'_2}, J'_1 = -J'_3 = A'_{\text{acc}} / T'_1 \end{array} \right\} \end{array} \right\} \quad (29)$$

where $a' = (T'_1 + T'_2/2)$, $b' = v_s(T'_1 + T'_2/2)$.

(b) Adjustment of feedrate phases for Type II (Fig. 5e–g).

For the scheduled jerk-limited feedrate profile without a constant feedrate zone, i.e. only $T_4 = 0$ (Fig. 5 e-g), the initial scheduled feedrate phases $T_i \quad (i=1, 2, 3, 5, 6, 7)$ are revised as $T'_i = \text{ceil}(T_i/T)T \quad (i=1, 2, 3, 5, 6, 7)$. Combing Eq. (20), the revised maximum feedrate (V'_{\max}), acceleration limits ($A'_{\text{acc}}, A'_{\text{dec}}$) and jerk limits (J'_1, J'_3, J'_5, J'_7) are evaluated as:

$$\left\{ \begin{array}{l} V'_{\max} = \frac{S_{\text{segment}} - b'}{a'} \\ A'_{\text{acc}} = \frac{V'_{\max} - v_s}{T'_1 + T'_2}, J'_1 = -J'_3 = \frac{A'_{\text{acc}}}{T'_1} \\ A'_{\text{dec}} = \frac{v_e - V'_{\max}}{T'_5 + T'_6}, J'_5 = -J'_7 = \frac{A'_{\text{dec}}}{T'_5} \end{array} \right\} \quad (30)$$

where $a' = (T'_1 + T'_5 + T'_2/2 + T'_6/2)$, $b' = v_s(T'_1 + T'_2/2) + v_e(T'_5 + T'_6/2)$.

When V'_{\max} is lower than or equal to the end feedrate v_e , V'_{\max} is not a feasible solution in the feedrate planning algorithm. To solve this problem, the maximum velocity (V'_{\max}) is updated, and the end velocity (v_e) and the feedrate profiles need to be further modified. Combing Eq. (18),

$$\left(\frac{v_s + V'_{\max}}{2} \right) (2T'_1 + T'_2) + T'_4 V'_{\max} = S_{\text{segment}} \quad (31)$$

where $T'_4 = T'_5 + T'_6 + T'_7$.

The updated V'_{\max} and the revised end velocity (v'_e) are evaluated as:

$$v'_e = V'_{\max} = \frac{S_{\text{segment}} - v_s(T'_1 + T'_2/2)}{T'_1 + T'_2/2 + T'_4} \quad (32)$$

Then, the acceleration and jerk limits are updated as:

$$\left\{ \begin{array}{l} A'_{\text{acc}} = \frac{V'_{\max} - v_s}{T'_1 + T'_2} \\ J'_1 = -J'_3 = A'_{\text{acc}} / T'_1 \end{array} \right\} \quad (33)$$

Hence, the updated feedrate phases and revised kinematic parameters are summarized as:

$$\left\{ \begin{array}{l} T'_1 = \text{ceil}\left(\frac{T_i}{T}\right)T \quad (i=1,2,3,5,6,7) \quad T'_4 = 0 \\ \text{when } V'_{\max} > v_e \quad \left\{ \begin{array}{l} V'_{\max} = \frac{S_{\text{segment}} - b'}{a'}, \\ A'_{\text{acc}} = \frac{V'_{\max} - v_s}{T'_1 + T'_2}, J'_1 = -J'_3 = \frac{A'_{\text{acc}}}{T'_1}, A'_{\text{dec}} = \frac{v_e - V'_{\max}}{T'_5 + T'_6}, J'_5 = -J'_7 = \frac{A'_{\text{dec}}}{T'_5} \end{array} \right. \\ \left. \begin{array}{l} T'_i = \text{ceil}\left(\frac{T_i}{T}\right)T \quad (i=1,2,3), \\ T'_4 = T'_5 + T'_6 + T'_7, T'_5 = T'_6 = T'_7 = 0 \\ v'_e = V'_{\max} = \frac{S_{\text{segment}} - v_s(T'_1 + T'_2/2)}{T'_1 + T'_2/2 + T'_4} \\ A'_{\text{acc}} = \frac{V'_{\max} - v_s}{T'_1 + T'_2}, J'_1 = -J'_3 = A'_{\text{acc}} / T'_1 \end{array} \right\} \end{array} \right\} \quad (34)$$

where $a' = (T'_1 + T'_5 + T'_2/2 + T'_6/2)$, $b' = v_s(T'_1 + T'_2/2) + v_e(T'_5 + T'_6/2)$.

(c) Adjustment of feedrate phases for Type III (Fig. 5h–j).

The feedrate phases $T_i \quad (i=1, 2, 3, 5, 6, 7)$ are revised as $T'_i = \text{ceil}(T_i/T)T \quad (i=1, 2, 3, 5, 6, 7)$. Assuming $T'_4 = 0$, the tool travel displacement in feedrate phases $T'_i \quad (i=1, 2, 3, 5, 6, 7)$ can be evaluated by Eq. (20) and denoted as S'_1 .

- When $S'_1 \leq S_{\text{segment}}$: Combing Eq. (20), the new phase T_4 is evaluated as:

$$T'_4 = \text{ceil}\left(\frac{S_{\text{segment}} - S'_1}{V_{\max}T}\right)T = \text{ceil}\left(\frac{S_{\text{segment}} - b'}{V_{\max}T} - \frac{a'}{T}\right)T \quad (35)$$

where $a' = (T'_1 + T'_5 + T'_2/2 + T'_6/2)$, $b' = v_s(T'_1 + T'_2/2) + v_e(T'_5 + T'_6/2)$.

Therefore, the modified maximum velocity (V'_{\max}), acceleration limits ($A'_{\text{acc}}, A'_{\text{dec}}$) and jerk limits (J'_1, J'_3, J'_5, J'_7) are evaluated as:

$$\left\{ \begin{array}{l} V'_{\max} = \frac{S_{\text{segment}} - b'}{T'_4 + a'} \\ A'_{\text{acc}} = \frac{V'_{\max} - v_s}{T'_1 + T'_2}, J'_1 = -J'_3 = \frac{A'_{\text{acc}}}{T'_1}, \\ A'_{\text{dec}} = \frac{v_e - V'_{\max}}{T'_5 + T'_6}, J'_5 = -J'_7 = \frac{A'_{\text{dec}}}{T'_5} \end{array} \right\} \quad (36)$$

where $a' = (T'_1 + T'_5 + T'_2/2 + T'_6/2)$, $b' = v_s(T'_1 + T'_2/2) + v_e(T'_5 + T'_6/2)$.

- When $S'_1 > S_{\text{segment}}$: The modified feedrate profile does not have a constant feedrate zone, therefore, the maximum velocity must be reduced as Eq. (30), and the updated feedrate phases and revised kinematic parameters are obtained as Eq. (34).

$$\begin{aligned} S'_1 \leq S_{\text{segment}} & \left\{ \begin{array}{l} T'_i = \text{ceil}(T_i/T)T \quad (i = 1, 2, 3, 5, 6, 7), T'_4 = \text{ceil}\left(\frac{S_{\text{segment}} - b'}{V_{\max} T} - \frac{a'}{T}\right)T \\ V'_{\max} = \frac{S_{\text{segment}} - b'}{T'_4 + a'}, A'_{acc} = \frac{V'_{\max} - v_s}{T'_1 + T'_2}, J'_1 = -J'_3 = \frac{A'_{acc}}{T'_1}, A'_{dec} = \frac{v_e - V'_{\max}}{T'_5 + T'_6}, J'_5 = -J'_7 = \frac{A'_{dec}}{T'_5} \end{array} \right. \\ S'_1 > S_{\text{segment}} & \text{Eq.(34)} \end{aligned} \quad (37)$$

Hence, the revised feedrate phases and kinematic parameters for Type III are summarized as:

where $a' = (T'_1 + T'_5 + T'_2/2 + T'_6/2)$, $b' = v_s(T'_1 + T'_2/2) + v_e(T'_5 + T'_6/2)$.

The flowchart of the proposed jerk-limited feedrate planning algorithm for $v_s < v_e$ is summarized in Fig. 6 with the following highlights:

- (1) The kinematic parameters of the current feedrate planning unit, including the start feedrate (v_s), end feedrate (v_e), feedrate, acceleration and jerk limits (F_c, A_{\max}, J_{\max}), and toolpath length of the feedrate planning unit (S_{segment}), are first set. Then the jerk-limited feedrate planning algorithm is implemented on the unit, i.e. $T_i (i = 1, \dots, 7)$ are calculated (Table 2).
- (2) When the feedrate profile does not have a deceleration zone (i.e. Type I, $T_5 = T_6 = T_7 = 0$), the initial scheduled feedrate phases $T_i (i = 1, 2, 3)$ are first revised by Eq. (21) as $T'_i = \text{ceil}(T_i/T)T$ ($i = 1, 2, 3$), then, the tool travel displacement in feedrate phases $T'_i (i = 1, 2, 3)$ (S'_{acc}) is obtained by Eq. (22). If $S'_{acc} < S_{\text{segment}}$ holds (Fig. 5a–b), the adjusted feedrate profile must have a constant feedrate phase T'_4 which is evaluated by Eq. (23). To ensure tool travel displacement in feedrate phases $T'_i (i = 1, \dots, 4)$ is shorter than or equal to S_{segment} , the maximum velocity (V_{\max}) on the current feedrate planning unit is revised as V'_{\max} by Eq. (25), leading to the revised kinematic parameters, including revised end feedrate (v'_e), acceleration limit (A'_{acc}) and jerk limits (J'_1, J'_3) which can be evaluated by Eq. (26). If $S'_{acc} \geq S_{\text{segment}}$ holds

(Fig. 5a–d), the adjusted feedrate profile does not have the constant feedrate phase T'_4 , i.e. $T'_4 = 0$. To ensure tool travel displacement in feedrate phases $T'_i (i = 1, \dots, 4)$ is no longer than S_{segment} , the maximum velocity (V_{\max}) and other kinematic parameters, including revised end feedrate (v'_e), acceleration limit (A'_{acc}) and jerk limits (J'_1, J'_3) are revised by Eq. (27) and Eq. (28) respectively. To sum up, the revised kinematic parameters and feedrate phases for the Type I feedrate profiles are summarized in Eq. (29).

- (3) When the feedrate profile has a deceleration zone but no constant feedrate zone, i.e. $T_4 = 0$ (Type II, Fig. 5e–g). The feedrate phases $T_i (i = 1, 2, 3, 5, 6, 7)$ are first revised as $T'_i = \text{ceil}(T_i/T)T (i = 1, 2, 3, 5, 6, 7)$, while the maximum velocity (V'_{\max}), acceleration limit (A'_{acc}) and jerk limits (J'_1, J'_3, J'_5, J'_7) are revised by Eq. (30). The revised V'_{\max} should be higher than v_e , otherwise, its value and v_e should be further modified as Eq. (32), and the acceleration and jerk limits are revised by Eq. (33). Hence, the complete revision equations for the Type II feedrate profiles are concluded in Eq. (34).
- (4) For a complete feedrate profile, i.e. a feedrate profile with an acceleration zone, a constant feedrate zone and a deceleration zone (Type III, Fig. 5h–j), the tool travel displacement S'_1 is calculated and compared against the toolpath length of the current feedrate planning unit S_{segment} . If $S'_1 \leq S_{\text{segment}}$ holds, then T_4 is revised by Eq. (35) and maximum velocity, acceleration and jerk limits are modified as Eq. (36). Otherwise, the maximum velocity must be reduced as Eq. (30), and the updated feedrate phases and revised kinematic parameters are obtained as Eq.

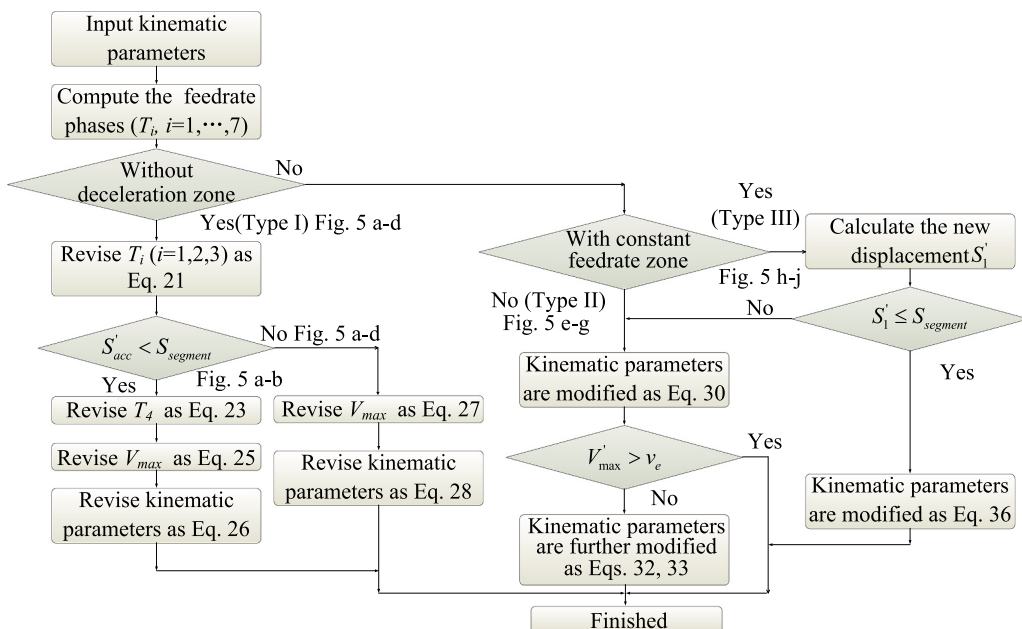


Fig. 6. Flowchart of modified jerk-limited feedrate planning algorithm ($v_s < v_e$).

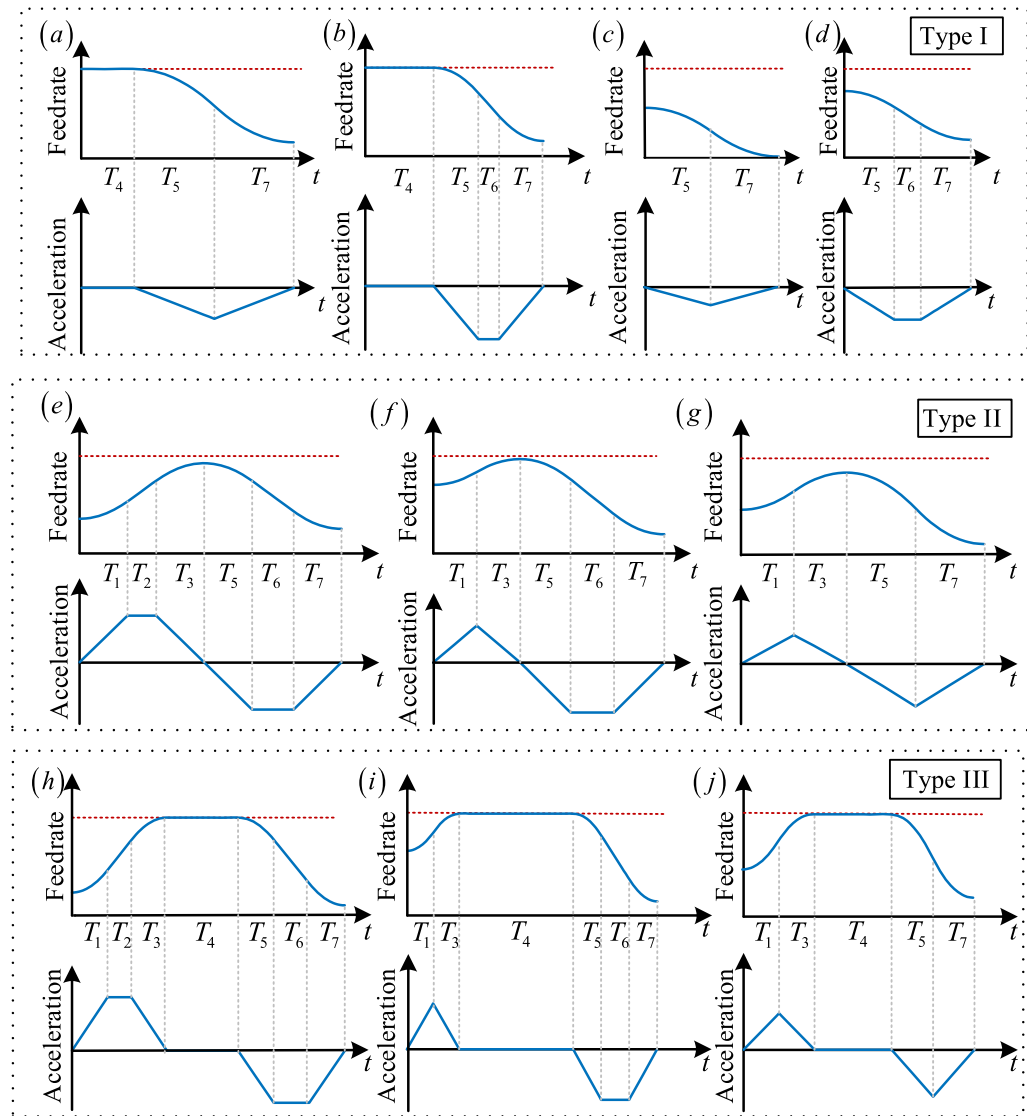


Fig. 7. Different feedrate profiles for $v_s > v_e$: (1–4) Type I; (5–7) Type II; (8–10) Type III.

(34). In summary, the revised kinematic parameters and feedrate phases for the Type III feedrate profiles are summarized in Eq. (37).

3.2. The start feedrate higher than the end feedrate (i.e. $v_s > v_e$)

Since the forward deceleration process can be considered as the inverse acceleration process, the adjustment of deceleration feedrate planning unit (Fig. 7) can be achieved similarly with the adjustment of acceleration feedrate planning unit (Section 3.1). The summary of the revised kinematic parameters and feedrate phases are obtained and summarized in Appendix D.

3.3. The start feedrate equal to the end feedrate (i.e. $v_s = v_e$)

For a feedrate profile consisting of only one constant feedrate zone, the initial scheduled values of T_i ($i = 1, 2, 3, 5, 6, 7$) and T_4 calculated by the jerk-limited feedrate planning algorithm (Table 2) are zeros and S_{Segment}/v_s respectively. Due to the integer adjustment for the interval time of the feedrate phases, the machining cycle time of the feedrate planning unit becomes longer, resulting in the modified maximum velocity being lower than the initial start feedrate v_s ($v_s \equiv v_e$). Hence, the

constant feedrate zone is transformed into a deceleration zone. Combing Eq. (19), assuming $T'_1 = 0$ and $T'_5 = T'_7 = \text{ceil}(T_4/(2T))T$, the re-modified maximum velocity (V'_{\max}) and end feedrate (v'_e) of the feedrate planning unit are evaluated as:

$$\left. \begin{aligned} V'_{\max} &= v_s \\ v'_e &= S_{\text{Segment}}/T'_5 - v_s \end{aligned} \right\} \quad (38)$$

Therefore, the maximum acceleration and maximum jerk are modified as:

$$\left. \begin{aligned} A'_{dec} &= (v'_e - v_s)/T'_5 \\ J'_5 &= -J'_7 = A'_{dec}/T'_5 \end{aligned} \right\} \quad (39)$$

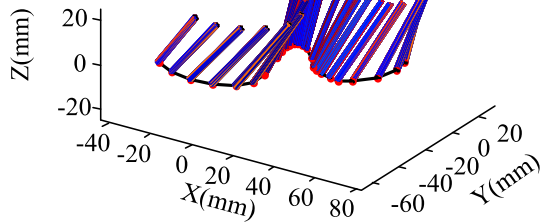
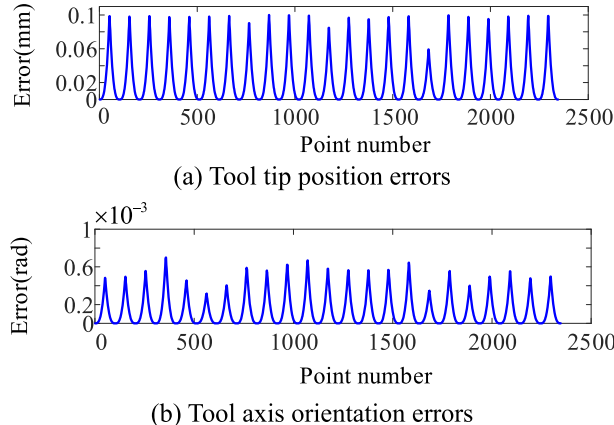
3.4. Optimization of computation efficiency

In the CNC system, one of the main functions of the feedrate planning modular is to calculate the tool travel displacement between the current and the next interpolation points. Since the CNC system is a real-time operating system, improving the computation efficiency of travel displacement is of great significance for improving system performance (reducing interpolation period) and ensuring the robustness of the sys-

Table 3

Comparison of computation load.

Feedrate phase	Addition and subtraction		Multiplication		Division		Improved efficiency F_i
	Table 1	Eq. 43	Table 1	Eq. 43	Table 1	Eq. 43	
T_1	$3T_a$	$3T_a$	$8T_m$	$4T_m$	$2T_d$	0	$F_1 = (4T_m + 2T_d)/(3T_a + 8T_m + 2T_d) > 0$
T_2	$5T_a$	$2T_a$	$6T_m$	$2T_m$	$2T_d$	0	$F_2 = (4T_m + 2T_d + 3T_a)/(5T_a + 6T_m + 2T_d) > 0$
T_3	$7T_a$	$5T_a$	$12T_m$	$6T_m$	$4T_d$	0	$F_3 = (6T_m + 4T_d + 2T_a)/(7T_a + 12T_m + 4T_d) > 0$
T_4	$3T_a$	0	$2T_m$	0	0	0	$F_4 = 1 > 0$
T_5	$5T_a$	$3T_a$	$8T_m$	$4T_m$	$2T_d$	0	$F_5 = (4T_m + 2T_d + 2T_a)/(5T_a + 8T_m + 2T_d) > 0$
T_6	$5T_a$	$2T_a$	$6T_m$	$2T_m$	$2T_d$	0	$F_6 = (4T_m + 2T_d + 3T_a)/(5T_a + 6T_m + 2T_d) > 0$
T_7	$7T_a$	$5T_a$	$12T_m$	$6T_m$	$4T_d$	0	$F_7 = (6T_m + 4T_d + 2T_a)/(7T_a + 12T_m + 4T_d) > 0$

**Fig. 8.** Five-axis tool path.**Fig. 9.** Tool path errors. (a) Tool tip position errors, (b) tool axis orientation errors.

tem. Based on the proposed feedrate profiles with multiples of the interpolation period, the computation efficiency of the travel displacement can be optimized by converting displacement calculation equations (Table 1) into difference equations. Assuming that the time interval $(k-1)T$ is shorter than T_i ($i = 1, \dots, 7$), and function $s(t)$ denotes the tool travel displacement at an arbitrary time t , then $s_i((k-1)T)$ represents the tool travel displacement within the time interval $(k-1)T$ in feedrate phase T_i . For feedrate phase T_1 , $s((k-1)T)$ is calculated as:

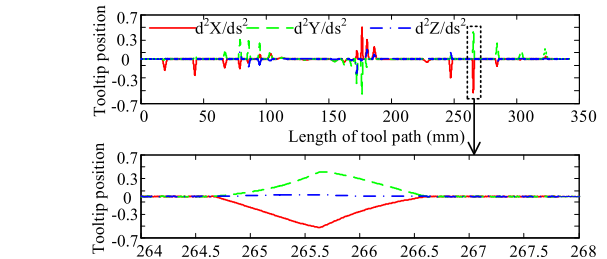
$$s((k-1)T) = v_s(k-1)T + \frac{1}{6}J_1(k-1)^3T^3 \quad (40)$$

Combing the tool travel displacement within the time interval kT :

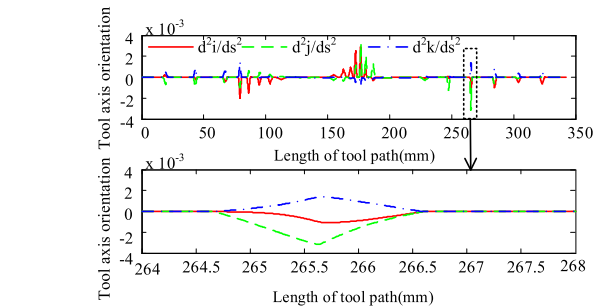
$$s(kT) = v_s kT + \frac{1}{6}J_1 k^3 T^3 \quad (41)$$

The computation of $s(kT)$ is simplified as:

$$s(kT) = s((k-1)T) + b_1 + a_1(3k^2 - 3k + 1) \quad (42)$$

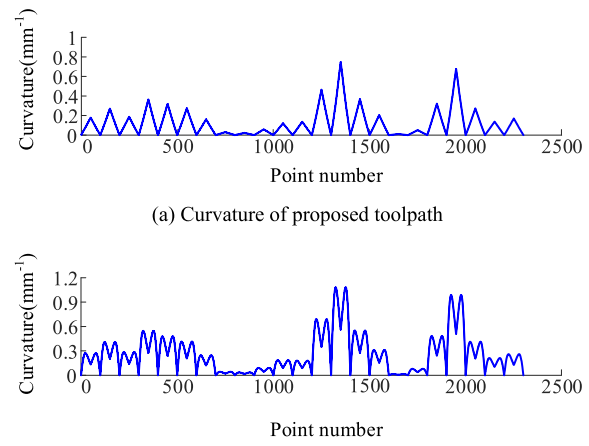


(a) The second geometrical derivative of the tooltip with respect to the displacement along the smoothed tool path



(b) The second geometrical derivative of the tool orientation with respect to the displacement along the smoothed tool path

Fig. 10. The second geometrical derivatives of the tooltip and tool orientation with respect to the displacement along the smoothed tool path. (a) The second geometrical derivative of the tooltip with respect to the displacement along the smoothed tool path. (b) The second geometrical derivative of the tool orientation with respect to the displacement along the smoothed tool path.

**Fig. 11.** Comparison of curvature along the smoothed tool path. (a) Curvature of proposed toolpath, (b) curvature of toolpath smoothed by algorithm I.

where $s(0) = 0, a_1 = J_1 T^3 / 6, b_1 = v_s T, k = 1, 2, \dots, (N_1 = T_1 / T)$.

Similarly, the tool travel displacement in the k th interpolation period is obtained for the different feedrate phases (T_i) as:

$$\begin{aligned} s((k-1)T) + b_1 + a_1(3k^2 - 3k + 1) & \quad k = 1, 2, \dots, (N_1 = T_1 / T) \\ s((k-1)T) + b_2 + a_2(2k-1) & \quad k = 1, 2, \dots, (N_2 = T_2 / T) \\ s((k-1)T) + b_3 + a_2(2k-1) - a_1(3k^2 - 3k + 1) & \quad k = 1, 2, \dots, (N_3 = T_3 / T) \\ s((k-1)T) + b_4 & \quad k = 1, 2, \dots, (N_4 = T_4 / T) \\ s((k-1)T) + b_5 + a_3(3k^2 - 3k + 1) & \quad k = 1, 2, \dots, (N_5 = T_5 / T) \\ s((k-1)T) + b_6 + a_4(2k-1) & \quad k = 1, 2, \dots, (N_6 = T_6 / T) \\ s((k-1)T) + b_7 + a_4(2k-1) - a_3(3k^2 - 3k + 1) & \quad k = 1, 2, \dots, (N_7 = T_7 / T) \end{aligned}$$

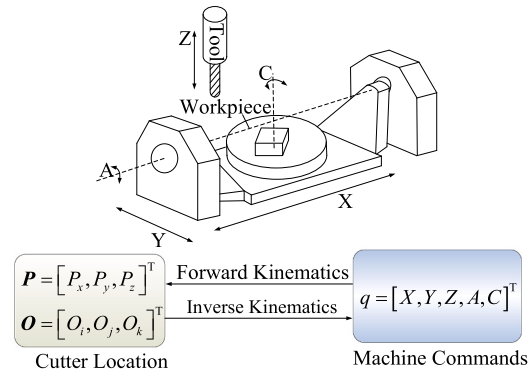
where $s(0)$ in the feedrate phase $T_i (i = 2, \dots, 7)$ is set to be equal to the tool travel displacement at the end of the previous feedrate phase, e.g., $s(0)$ in the feedrate phase T_2 is set to be equal to $s(N_1 T)$.

The constants $a_i (i = 1, \dots, 4)$ and $b_i (i = 1, \dots, 7)$ can be evaluated during the initialization and simply added recursively during real-time interpolation point calculation. Therefore, the computation load of tool travel displacement in each interpolation period is reduced. The computation load of the optimized tool travel displacement calculation

method (Eq. (43)) is compared against that of the previous calculation method (Table 1) in Table 3. T_a , T_m and T_d represent the instruction cycle time of single addition/subtraction, multiplication and division respectively. In the feedrate phase T_1 , the computation time is reduced

$$\left. \begin{aligned} a_1 &= J_1 T^3 / 6, b_1 = v_s T \\ a_2 &= A_{acc} T^2 / 2, b_2 = v_1 T \\ b_3 &= v_2 T \\ b_4 &= v_3 T \\ a_3 &= J_5 T^3 / 6, b_5 = v_4 T \\ a_4 &= A_{dec} T^2 / 2, b_6 = v_5 T \\ b_7 &= v_6 T \end{aligned} \right\} \quad (43)$$

from $(3T_a + 8T_m + 2T_d)$ in Table 1 to $(3T_a + 4T_m)$ in Eq. (43). Since the instruction cycle time of multiply/division operation is much longer than that of the addition/subtraction operation, the computation load of tool travel displacement is reduced, and the efficiency is improved by $F_1 = (4T_m + 2T_d) / (3T_a + 8T_m + 2T_d) > 0$. Similarly, according to the different feedrate phases (T_i), the computation efficiency of tool travel displacement in different interpolation periods is also improved resulting in improved computation efficiency of the feedrate planning



(a) Five-axis machining center and machine tool kinematics



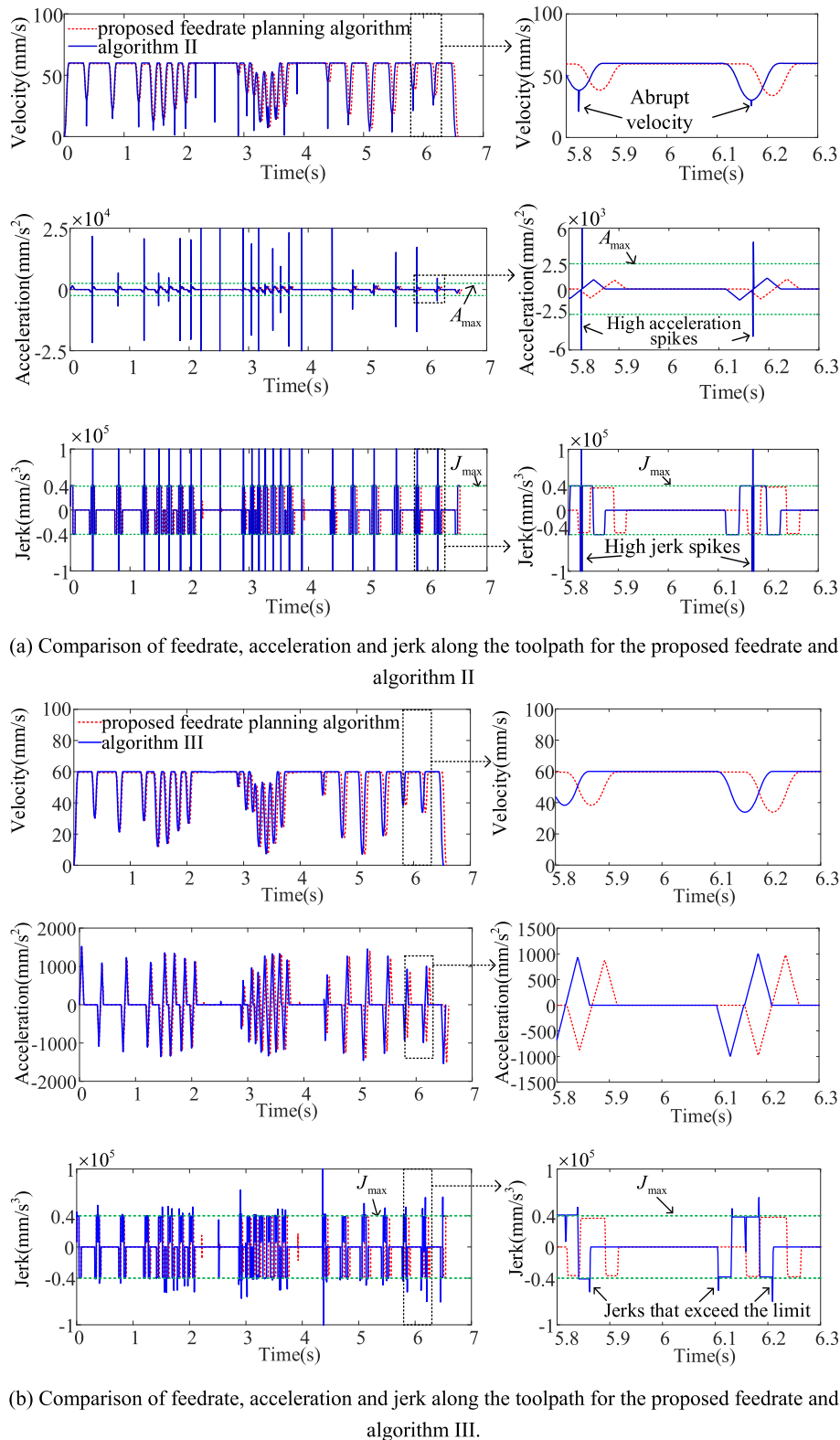
(b) Golding GJ430 CNC

Fig. 12. Experimental platform. (a) Five-axis machining center and machine tool kinematics, (b) Golding GJ430 CNC.

Table 4

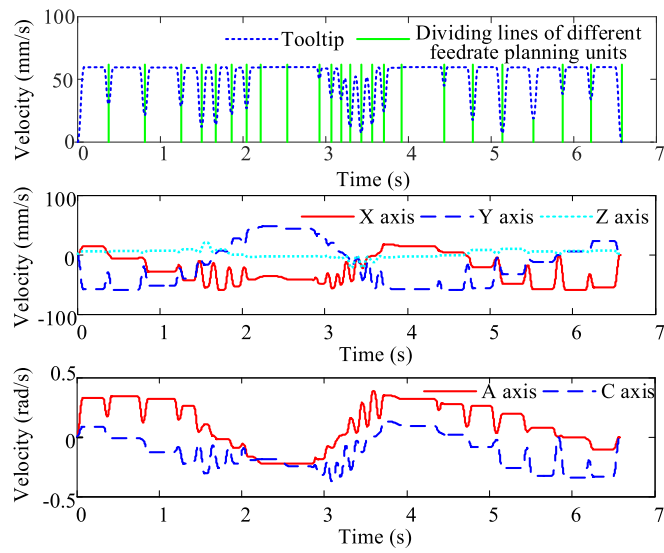
Velocity, acceleration and jerk limits of machine drives.

	X drive	Y drive	Z drive	A drive	C drive
Maximum velocity	150 mm/s	150 mm/s	150 mm/s	2 rad/s	5 rad/s
Maximum acceleration	2500 mm/s ²	2500 mm/s ²	2500 mm/s ²	30 rad/s ²	50 rad/s ²
Maximum jerk	40,000 mm/s ³	40,000 mm/s ³	40,000 mm/s ³	500 rad/s ³	500 rad/s ³

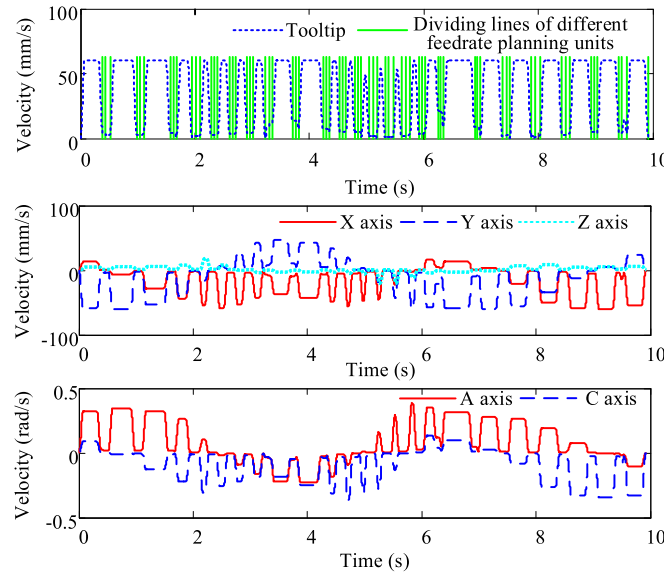


(b) Comparison of feedrate, acceleration and jerk along the toolpath for the proposed feedrate and algorithm III.

Fig. 13. Comparison of feedrate, acceleration and jerk along the toolpath. (a) Comparison of feedrate, acceleration and jerk along the toolpath for the proposed feedrate and algorithm II, (b) comparison of feedrate, acceleration and jerk along the toolpath for the proposed feedrate and algorithm III.



(a) Feedrate commands of tooltip and five axes along proposed toolpath



(b) Feedrate commands of tooltip and five axes along algorithm I toolpath

Fig. 14. Feedrate commands of tooltip and five axes along proposed toolpath and algorithm I toolpath. (a) Feedrate commands of tooltip and five axes along proposed toolpath, (b) feedrate commands of tooltip and five axes along algorithm I toolpath.

algorithm (Table 3).

4. Simulation and experimental results

The proposed five-axis toolpath interpolation algorithm with Bezier splines and feedrate profile that has an integer multiple of the interpolation period, has been validated with simulations and experiments following a five-axis toolpath with 24 segments (Fig. 8). The user-defined tool tip position and orientation error tolerances are 0.1 mm and 0.001 rad, respectively. The five-axis toolpath (Fig. 8) is first smoothed by the proposed corner smoothing algorithm (Section 2). As

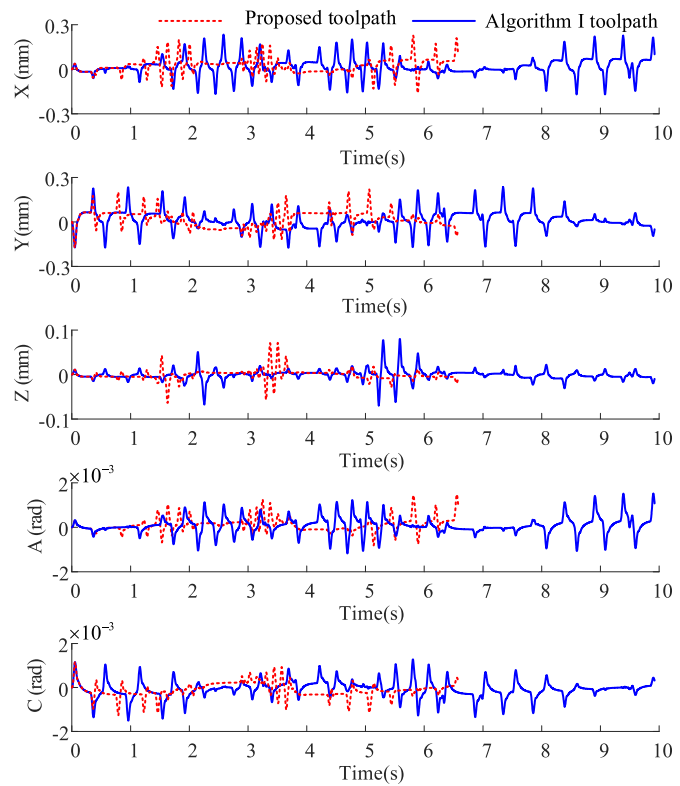


Fig. 15. Comparison of tracking errors.

shown in Fig. 9, the tooltip position and tool axis orientation errors are kept within the set tolerances of 0.1 mm and 0.001 rad, respectively.

The second geometrical derivatives of the tooltip and tool orientation with respect to the displacement along the smoothed tool path are presented in Fig. 10. As an arbitrary sample, a zoomed view of the smoothed tool path around the 20th point is illustrated and shows that the first and second geometrical derivatives match at the path junctions, i.e., the smoothed toolpath has G^2 continuity.

The proposed G^2 continuous toolpath with monotonic curvature is compared against the art paths without monotonic curvature optimization (algorithm I). As shown in Fig. 11, the proposed tool path has 23 extreme points on the curvature profile, while the number of curvature points of the algorithm I toolpath is twice that of the proposed algorithm. Since the smoothed toolpath is divided into different feedrate planning units as per the extreme curvature, i.e., each toolpath segment between two adjacent extreme curvatures is defined as a single feedrate planning unit, the monotonic curvature contributes to reducing the number of feedrate planning units.

4.1. Optimized computation efficiency

The computation time of tool travel displacement is compared for the proposed jerk-limited feedrate profile with integer multiples of the interpolation period and the profile without integer multiples of the interpolation period (algorithm II). These algorithms are developed in the Matlab environment, and the tool travel displacement is generated at 1 ms time intervals (i.e. interpolation periods). The computation time of tool travel displacement in all interpolation periods with an AMD Ryzen 75800H 3.2 GHz is 2.81 ms and 4.98 ms for the proposed feedrate profile

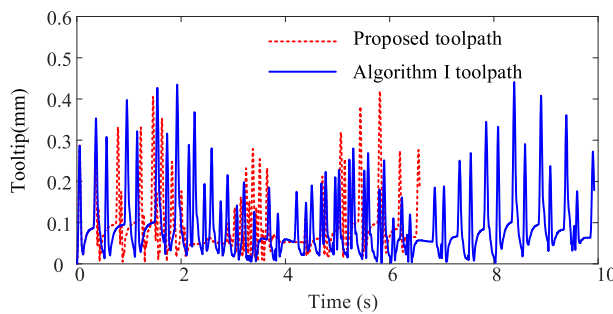


Fig. 16. Comparison of contour errors.

Table 5

Measured maximum axis tracking errors (Fig. 15) and tooltip contour errors (Fig. 16) for proposed algorithm and algorithm I.

Smoothing method	Measured maximum axis tracking errors and tooltip contour errors											
	t (s)	X (μm)	t (s)	Y (μm)	t (s)	Z (μm)	t (s)	A (mrad)	t (s)	C (mrad)	t (s)	Tooltip (μm)
Proposed algorithm	5.811	228	5.063	219	3.507	71	6.555	1.478	0.054	1.157	5.812	419
Algorithm I	2.583	234	7.343	235	5.586	80	9.901	1.518	5.807	1.281	8.390	440

and profile of algorithm II, respectively. Because the travel displacement is calculated by the difference equations (Eq. (43)) rather than the displacement calculation equations (Table 1), the proposed feedrate profile reduces the computation time by about 43.57 % than algorithm II. The improved computation efficiency will help to improve system performance (reduce interpolation period) and ensure system robustness.

4.2. Elimination of feedrate fluctuation within the feedrate planning units

Coupled with the proposed feedrate, algorithm II and the algorithm presented by Du et al. [47] (algorithm III) respectively, the position commands are generated at 1 ms time intervals along the proposed toolpath and sent to machine drives. The trajectory tracking experiments are carried out on a VMC2100B 5-axis machining center (Fig. 12 (a)) whose kinematical characteristics are given in Table 4. The feedrate, acceleration and jerk limits of the machine tool drives along the toolpath are 60 mm/s, 2500 mm/s² and 40,000 mm/s³, respectively. The machine is controlled by a Golding GJ430 CNC developed by Shenyang CASNC Technology Co., Ltd. (Fig. 12(b)), which has a debugging modular that allows direct control of the movement with position command.

Combining the axis displacements measured from the encoders of the machine, the tooltip velocity, i.e. the first order derivative of the tooltip displacements, is evaluated by the following digital differentiation.

$$f = \frac{dD_{is}}{dt} = \frac{D_{is}(t_{i+1}) - D_{is}(t_i)}{\Delta t} \quad (44)$$

where $\Delta t = 1$ ms is the axis position control loop closure time; $X(t_i)$, $Y(t_i)$ and $Z(t_i)$ are the axis position measured at $t_i = i\Delta t$, respectively; D_{is} is the displacement in the i -th axis position control loop closure time, i.e.

$$D_{is}(t_i) = \sqrt{(X(t_{i+1}) - X(t_i))^2 + (Y(t_{i+1}) - Y(t_i))^2 + (Z(t_{i+1}) - Z(t_i))^2}. \quad (45)$$

Similarly, the acceleration and jerk are evaluated as

$$\left. \begin{aligned} a &= \frac{d^2D_{is}}{dt^2} = \frac{D_{is}(t_{i+2}) - 2D_{is}(t_{i+1}) + D_{is}(t_i)}{\Delta t^2} \\ j &= \frac{d^3D_{is}}{dt^3} = \frac{D_{is}(t_{i+3}) - 3D_{is}(t_{i+2}) + 3D_{is}(t_{i+1}) - D_{is}(t_i)}{\Delta t^3} \end{aligned} \right\} \quad (45)$$

The tooltip velocity, acceleration and jerk of the proposed feedrate planning algorithm, algorithm II and algorithm III are compared in Fig. 13. In CNC machining, the tool's travel time must only consist of integer multiples of the interpolation period. Because algorithm II does not adjust the kinematic parameters to generate a feedrate profile with an integer multiple of the interpolation period, the displacement discarded in the rounding has to be travelled in an independent period, leading to feedrate fluctuation and abrupt change of acceleration and jerk within the last interpolation period of each feedrate planning unit (Fig. 13(a)). Thanks to the interpolation period rounding method and variable-jerk compensation strategy, algorithm III can quantize each feedrate phase with integer multiples of interpolation periods and eliminate high acceleration/jerk spikes. However, the discretization-based arc length compensation strategy still generates jerks that exceed the limit (Fig. 13(b)). Based on the detailed mathematical formulations of the modified jerk-limited feedrate planning algorithm, the proposed feedrate profile not only has integer multiples of the interpolation period, but also constrains the acceleration and jerk under the limits, hence eliminates feedrate fluctuation within the feedrate planning units, resulting in smoother feedrate, acceleration and jerk profiles. The smooth feedrate and reduced acceleration and jerk help to avoid excitation of machine tool's structural modes hence improve tracking accuracy during high-speed positioning.

4.3. Reduction of feedrate fluctuation along the smoothed toolpath

Combining the proposed feedrate planning algorithm, the feedrate commands of the tooltip and five axes of the machine tools are generated along the proposed toolpath and algorithm I toolpath, respectively, and the results are shown in Fig. 14. Since the proposed toolpath has fewer feedrate planning units, it reduces the feedrate fluctuation compared to the algorithm I toolpath. The machining cycles for the proposed toolpath and algorithm I toolpath are 6.577 s and 9.923 s, respectively, which indicates that the proposed algorithm significantly improves the machining efficiency by about 33.7 %. Then, the CNC trajectories are generated at 1 ms time intervals along the proposed toolpath and the algorithm I toolpath, respectively. These C^2 continuous position commands are sent to five axes (X, Y, Z, A, C) of the five-axis machining center using its inverse kinematics model. Their effect on the smooth

motion and contour machining can be observed in the measured tracking error history of the five axes of the machine tool in Fig. 15.

Since the geometric commands are much smooth in the proposed toolpath, the resulting position commands are also smoother than the algorithm I toolpath. The smoother position commands have lower frequency content, leading to better tracking performance of the servo drives with limited bandwidth (Fig. 15), and better contour accuracy (Fig. 16). The magnitudes of the largest tracking errors of the axes and the largest tooltip contour errors along the toolpath are compared in Table 5, which indicates that the proposed toolpath can significantly reduce the maximum tracking errors and tooltip contour errors than algorithm I tool path.

5. Conclusion

A smooth interpolation method of the five-axis tool path with less feedrate fluctuation and higher computation efficiency is presented. Compared with the existing interpolation methods in the literature, the proposed toolpath smoothing algorithm can keep the monotonic curvature, hence reduces the number of feedrate planning units, leading to less fluctuation of the scheduled feedrate profile along the toolpath and improved machining efficiency; the proposed feedrate planning algorithm ensures the time interval of each feedrate phase of an arbitrary feedrate planning unit has an integer multiple of the interpolation period, hence eliminates the feedrate fluctuation within the feedrate planning units and improves the computation efficiency of position commands in each interpolation period. As demonstrated in five-axis machining simulations and experiments, the proposed feedrate planning algorithm can generate a feedrate profile with an integer multiple of the interpolation period, hence eliminates the feedrate fluctuation within the feedrate planning units; the proposed toolpath smoothing algorithm can constrain path error within the tolerance, synchronize the motion of tooltip and orientation, and reduce the fluctuation of scheduled feedrate profile along the toolpath and improve the machining efficiency. Coupled the proposed feedrate planning algorithm, the proposed tool paths lead to smaller tracking and contour errors which improve the machining accuracy.

Appendix A

To synchronize the tool orientation and tip position, $(d\text{Ori}/ds, d^2\text{Ori}/ds^2)$ must be continuous at tip position $P_{k,0}^b$.

(a) The $d\text{Ori}/ds^2$ of the transition Bezier curve $B_k^b(u)$ at its end point ($u = 1$) is evaluated as:

$$\frac{d\text{Ori}_k(u=1)}{ds} = \frac{C'(1) - C''(1)}{\|C'(1) - C''(1)\|} \frac{1}{\|C''(1)\|} \quad (\text{A.1})$$

Since

$$\left. \begin{aligned} C'(1) &= 3(P'_{k,0} - P'_{k,1}) \\ C''(1) &= 3(P''_{k,0} - P''_{k,1}) \end{aligned} \right\} \quad (\text{A.2})$$

Eq. (A.1) can be reorganized as:

Funding

This work was sponsored by National Natural Science Foundation of China-NSFC (Grant No. 62002308); International Science and Technology Cooperation Program in Yantai City (Grant No. 2023YTKXGH001); 2023 Innovation capability improvement project of small and medium-sized scientific and technological enterprises in Shandong Province (Grant No. 2023TSGC0853); and Fundamental Research Projects of Science & Technology Innovation and development Plan in Yantai City (Grant No. 2022JCYJ036).

CRediT authorship contribution statement

Shujie Sun: Conceptualization, Methodology, Software, Validation, Formal analysis, Resources, Writing – original draft, Writing – review & editing, Supervision, Project administration, Funding acquisition. **Peng Zhao:** Methodology, Writing – original draft, Software, Formal analysis. **Tao Zhang:** Writing – original draft, Software, Validation. **Beibei Li:** Software, Validation, Resources, Writing – review & editing, Supervision, Funding acquisition. **Dong Yu:** Resources, Writing – review & editing, Supervision.

Declaration of competing interest

The authors declare that they have no known competing financial interests or personal relationships that could have appeared to influence the work reported in this paper.

Data availability

No data was used for the research described in the article.

Acknowledgements

The author thanks Shenyang CASNC Technology Co., Ltd. and the National Engineering Research Center for High-End CNC, Shenyang Institute of Computing Technology, Chinese Academy of Sciences, for supporting the experimental portion of this work.

$$\frac{dOri_k(u=1)}{ds} = \frac{3(P_{k,0}^t - P_{k,1}^t) - 3(P_{k,0}^b - P_{k,1}^b)}{\|P_{k,0}^t - P_{k,1}^b\|} \frac{1}{\|3(P_{k,0}^b - P_{k,1}^b)\|} = \frac{\frac{P_{k,0}^t - P_{k,1}^t}{P_{k,0}^b - P_{k,1}^b} - 1}{\|P_{k,0}^t - P_{k,1}^b\|} \frac{P_{k,0}^b - P_{k,1}^b}{\|P_{k,0}^b - P_{k,1}^b\|} \quad (\text{A.3})$$

For the linear segment $P_{k,0}^b Q_{i+1}^b$, the first derivative of tool axis orientation at its starting point $P_{k,0}^b$ ($u = 0$) is evaluated as:

$$\frac{dOri_{line,k}(u=0)}{ds} = \frac{C'(0) - C^{b'}(0)}{\|C'(0) - C^{b'}(0)\|} \frac{1}{\|C^{b'}(0)\|} \quad (\text{A.4})$$

Since

$$\begin{cases} C'(0) = \beta(Q_{i+1}^t - P_{k,0}^t)/(2(\alpha + \beta + 1)) \\ C^{b'}(0) = \beta(Q_{i+1}^b - P_{k,0}^b)/(2(\alpha + \beta + 1)) \end{cases} \quad (\text{A.5})$$

Eq. (A.4) can be reorganized as:

$$\frac{dOri_{line,k}(u=0)}{ds} = \frac{(Q_{i+1}^t - P_{k,0}^t) - (Q_{i+1}^b - P_{k,0}^b)}{\|P_{k,0}^t - P_{k,0}^b\|} \frac{1}{\|Q_{i+1}^b - P_{k,0}^b\|} = \frac{\frac{Q_{i+1}^t - P_{k,0}^t}{Q_{i+1}^b - P_{k,0}^b} - 1}{\|P_{k,0}^t - P_{k,0}^b\|} \frac{Q_{i+1}^b - P_{k,0}^b}{\|Q_{i+1}^b - P_{k,0}^b\|} \quad (\text{A.6})$$

The $dOri/ds$ must match at the connection point $P_{k,0}^b$ (i.e. $dOri_k(u=1)/ds = dOri_{line,k}(u=0)/ds$), which yields:

$$\frac{P_{k,0}^t - P_{k,1}^t}{P_{k,0}^b - P_{k,1}^b} = \frac{Q_{i+1}^t - P_{k,0}^t}{Q_{i+1}^b - P_{k,0}^b} \quad (\text{A.7})$$

Therefore,

$$\frac{\|P_{k,1}^t P_{k,0}^t\|}{\|P_{k,1}^b P_{k,0}^b\|} = \frac{\|P_{k,0}^t Q_{i+1}^t\|}{\|P_{k,0}^b Q_{i+1}^b\|} \quad (\text{A.8})$$

Considering,

$$\begin{cases} \|P_{k,0}^t - P_{k,1}^t\|(\alpha + \beta + 1) = \|Q_i^t P_{k,0}^t\| \\ \|P_{k,0}^b - P_{k,1}^b\|(\alpha + \beta + 1) = \|Q_i^b P_{k,0}^b\| \end{cases} \quad (\text{A.9})$$

Hence,

$$\frac{\|Q_i^t P_{k,0}^t\|}{\|Q_i^b P_{k,0}^b\|} = \frac{\|Q_i^t P_{k,0}^t\| + \|P_{k,0}^t Q_{i+1}^t\|}{\|Q_i^b P_{k,0}^b\| + \|P_{k,0}^b Q_{i+1}^b\|} = \frac{\|Q_i^t Q_{i+1}^t\|}{\|Q_i^b Q_{i+1}^b\|} \quad \text{i.e.} \quad \frac{\|Q_i^t P_{k,0}^t\|}{\|Q_i^b P_{k,0}^b\|} = \frac{\|Q_i^t Q_{i+1}^t\|}{\|Q_i^b Q_{i+1}^b\|} \quad (\text{A.10})$$

(b) The first and second derivatives of the transition Bezier curve $B_k^b(u)$ at its end point ($u = 1$) are collinear, which yields:

$$u_{ss}^b = -\frac{\langle C^{b'}(1), C^{b''}(1) \rangle}{\|C^{b'}(1)\|^4} = 0 \quad (\text{A.11})$$

Therefore, the d^2Ori/ds^2 is simplified as:

$$\frac{d^2Ori_k(u=1)}{ds^2} = \frac{1}{\|C'(u) - C^b(u)\|} (C'(u) - C^{b'}(u)) (u_s^b)^2 \quad (\text{A.12})$$

Since the second derivatives at its ending point $P_{k,0}^b$ ($u = 1$) are evaluated as:

$$\begin{cases} C'(1) = 6(P_{k,0}^t - 2P_{k,1}^t + P_{k,2}^t) = 6(1 - \alpha/\beta)(P_{k,0}^t - P_{k,1}^t) \\ C^{b'}(1) = 6(P_{k,0}^b - 2P_{k,1}^b + P_{k,2}^b) = 6(1 - \alpha/\beta)(P_{k,0}^b - P_{k,1}^b) \end{cases} \quad (\text{A.13})$$

Eq. (A.12) can be reorganized as:

$$\begin{aligned}
\frac{d^2Ori_k(u=1)}{ds^2} &= \frac{1}{\|C^t - C^b\|} (C^{t''} - C^{b''}) (u_s^b)^2 \\
&= \frac{6(1-\alpha/\beta)}{\|P_{k,0}^t - P_{k,0}^b\|} \left((P_{k,0}^t - P_{k,1}^t) - (P_{k,0}^b - P_{k,1}^b) \right) \left(\frac{1}{\|3(P_{k,0}^b - P_{k,1}^b)\|} \right)^2 \\
&= \frac{2(1-\alpha/\beta) \left(\frac{(P_{k,0}^t - P_{k,1}^t)}{(P_{k,0}^b - P_{k,1}^b)} - 1 \right)}{3\|P_{k,0}^t - P_{k,0}^b\| \|P_{k,0}^b - P_{k,1}^b\|^2} (P_{k,0}^b - P_{k,1}^b)
\end{aligned} \tag{A.14}$$

For the linear segment $P_{k,0}^b Q_{i+1}^b$, the second derivatives at its starting point $P_{k,0}^b$ ($u = 0$) are evaluated as:

$$\left. \begin{aligned}
C^{t'}(0) &= 6 \frac{(Q_{i+1}^t - P_{k,0}^t)}{2(\alpha + \beta + 1)} (\alpha - \beta) = \frac{3(Q_{i+1}^t - P_{k,0}^t)}{(\alpha + \beta + 1)} (\alpha - \beta) \\
C^{b'}(0) &= 6 \frac{(Q_{i+1}^b - P_{k,0}^b)}{2(\alpha + \beta + 1)} (\alpha - \beta) = \frac{3(Q_{i+1}^b - P_{k,0}^b)}{(\alpha + \beta + 1)} (\alpha - \beta)
\end{aligned} \right\} \tag{A.15}$$

Therefore, d^2Ori/ds^2 is evaluated as:

$$\begin{aligned}
\frac{d^2Ori_{line,k}(u=0)}{ds^2} &= \frac{1}{\|C^t(0) - C^b(0)\|} (C^{t'}(0) - C^{b'}(0)) (u_s^b)^2 \\
&= \frac{3(\alpha - \beta)}{\|P_{k,0}^t - P_{k,0}^b\| (\alpha + \beta + 1)} \left((Q_{i+1}^t - P_{k,0}^t) - (Q_{i+1}^b - P_{k,0}^b) \right) \left(\frac{1}{\|3(Q_{i+1}^b - P_{k,0}^b)\beta/(2(\alpha + \beta + 1))\|} \right)^2 \\
&= \frac{4(\alpha - \beta)(\alpha + \beta + 1)}{3\beta^2 \|P_{k,0}^t - P_{k,0}^b\| \|Q_{i+1}^b - P_{k,0}^b\|^2} \left(\frac{(Q_{i+1}^t - P_{k,0}^t)}{(Q_{i+1}^b - P_{k,0}^b)} - 1 \right) (Q_{i+1}^b - P_{k,0}^b)
\end{aligned} \tag{A.16}$$

The d^2Ori/ds^2 must match at the connection point $P_{k,0}^b$ (i.e. $d^2Ori_k(u=1)/ds = d^2Ori_{line,k}(u=0)/ds$),

$$\frac{(1-\alpha/\beta)}{\|P_{k,0}^b - P_{k,1}^b\|} = \frac{2(\alpha - \beta)(\alpha + \beta + 1)}{\beta^2 \|Q_{i+1}^b - P_{k,0}^b\|} \tag{A.17}$$

which yields $\alpha = \beta$.

Appendix B

By substituting m and n in to Eq. (13),

$$\kappa' = \frac{-\Gamma(\alpha, \theta, u)}{6l_1 n^{5/2}}, u \in [0, 1] \tag{B.1}$$

where

$$\Gamma(\alpha, \theta, u) = 2\alpha \cos \theta \sin \theta [\alpha^2 u^2 (u-2)^2 + \cos^2(u-1)^2 p_1] + p_2, \theta \in [0, \pi/2) \tag{B.2}$$

$$p_1 = [(u-1)^2 - 2\alpha u(u-2)] = u^2(1-2\alpha) + 2u(2\alpha-1) + 1 \geq 0 \tag{B.3}$$

$$p_2 = 3\cos \theta \sin \theta \alpha(1-u)(q_1 + q_2) \tag{B.4}$$

$$q_1 = \alpha^2 2u(u-2)^2 + 2\alpha^2 u^2(u-2) = 2\alpha^2 u(u-2)2(u-1) \geq 0;$$

$$q_2 = \cos^2 \theta q_3 + \cos^2 \theta q_4,$$

$$q_3 = 2(u-1)[(u-1)^2 - 2\alpha u(u-2)] \geq 0, \quad q_4 = (u-1)^2[2(u-1) - 2\alpha(u-2) - 2\alpha u].$$

Assume $g(u) = q_1 + q_2$, i.e.

$$g(u) = q_1 + q_2 = 2(u - 1)g_1 \quad (\text{B.5})$$

where $g_1(u) = 2u^2[\cos^2\theta(1 - 2\alpha) + \alpha^2] + 4u[\cos^2\theta(2\alpha - 1) - \alpha^2] + 2\cos^2\theta(1 - \alpha)$ holds and the distribution of $g_1(u)$ on the parameter interval $u \in [0, 1]$ is illustrated in Fig. B.1.

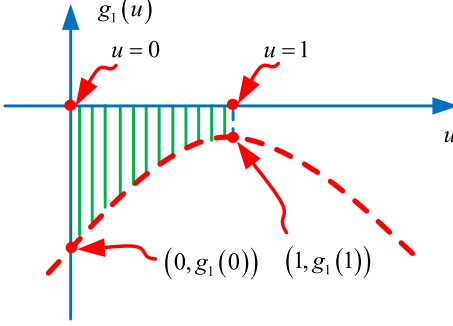


Fig. B.1. Distribution of $g_1(u)$ on the parameter interval $u \in [0, 1]$.

Since $g_1(0) = 2(1 - \alpha)\cos^2\theta \leq 0$ and $g_1(1) = 2\alpha(-\alpha + \cos^2\theta) \leq 0$ hold, the value of $g_1(u)$ on the parameter interval $u \in [0, 1]$ is zero or smaller. Hence, $g(u)$ (Eq. (B.5)) is zero or greater.

Combing Eqs. (B.3)–(B.4), $\Gamma(\alpha, \theta, u)$ (Eq. (B.2)) is no smaller than zero. Hence, $\kappa' \leq 0$, i.e. spline curve $B_k^b(u)$ has monotonically decreasing curvature.

Appendix C

To synchronize the tool orientation and tip position, $(d\text{Ori}/ds, d^2\text{Ori}/ds^2)$ must be continuous at tip position $P_{k,3}^b$.

(a) The $d\text{Ori}/ds$ of the transition Bezier curve $B_k^b(u)$ at its starting point ($u = 0$) is evaluated as:

$$\frac{d\text{Ori}_k(u=0)}{ds} = \frac{C'(0) - C^{b'}(0)}{\|C'(0) - C^{b'}(0)\|} \frac{1}{\|C^{b'}(0)\|} \quad (\text{C.1})$$

Since

$$\left. \begin{aligned} C'(0) &= 3(P'_{k,2} - P'_{k,3}) \\ C^{b'}(0) &= 3(P^b_{k,2} - P^b_{k,3}) \end{aligned} \right\} \quad (\text{C.2})$$

Eq. (C.1) can be reorganized as:

$$\frac{d\text{Ori}_k(u=0)}{ds} = \frac{3(P'_{k,2} - P'_{k,3}) - 3(P^b_{k,2} - P^b_{k,3})}{\|P'_{k,3} - P^b_{k,3}\|} \frac{1}{\|3(P^b_{k,2} - P^b_{k,3})\|} = \frac{\frac{P'_{k,2} - P'_{k,3}}{P^b_{k,2} - P^b_{k,3}} - 1}{\|P'_{k,3} - P^b_{k,3}\|} \frac{P^b_{k,2} - P^b_{k,3}}{\|P^b_{k,2} - P^b_{k,3}\|} \quad (\text{C.3})$$

Similarly, $d\text{Ori}/ds$ of the transition Bezier curve $B_{k-1}^b(u)$ at its end point ($u = 1$) is evaluated as:

$$\frac{d\text{Ori}_{k-1}(u=1)}{ds} = \frac{3(P'_{k-1,3} - P'_{k-1,2}) - 3(P^b_{k-1,3} - P^b_{k-1,2})}{\|P'_{k-1,3} - P^b_{k-1,3}\|} \frac{1}{\|3(P^b_{k-1,3} - P^b_{k-1,2})\|} = \frac{\frac{P'_{k-1,3} - P'_{k-1,2}}{P^b_{k-1,3} - P^b_{k-1,2}} - 1}{\|P'_{k-1,3} - P^b_{k-1,3}\|} \frac{P^b_{k-1,3} - P^b_{k-1,2}}{\|P^b_{k-1,3} - P^b_{k-1,2}\|} \quad (\text{C.4})$$

Since $P_{k-1,3}^b \equiv P_{k,3}^b$ is the middle point of $P_{k-1,2}^b$ and $P_{k,2}^b$, $P_{k,2}^b - P_{k,3}^b = P_{k-1,3}^b - P_{k-1,2}^b$ holds. Similarly, $P_{k,2}^t - P_{k,3}^t = P_{k-1,3}^t - P_{k-1,2}^t$ holds. Combing $P_{k,3}^b = P_{k-1,3}^b$ and $P_{k,3}^t = P_{k-1,3}^t$, Eq. (C.3) is equal to Eq. (C.4), i.e. $d\text{Ori}_k(u=0)/ds = d\text{Ori}_{k-1}(u=1)/ds$.

(b) In Fig. 3(a), assuming that points $(Q_{i,pre}^b, Q_{i,next}^b)$ are on the linear segments $(Q_{i-1}^b Q_i^b, Q_i^b Q_{i+1}^b)$, respectively; $(P_{k-1,1}^b, P_{k,2}^b)$ are the middle points of $(P_{k-1,1}^b Q_{i,pre}^b, P_{k,1}^b Q_{i,next}^b)$, respectively.

The $d^2\text{Ori}/ds^2$ of the transition Bezier curve $B_k^b(u)$ at its starting point ($u = 0$) is evaluated as:

$$\frac{d^2Ori_k(u=0)}{ds} = \frac{1}{\|C'(0) - C^b(0)\|} \left[(C^{'}(0) - C^{b'}(0)) (u_s^b)^2 + (C^{'}(0) - C^{b'}(0)) u_{ss}^b \right] \quad (\text{C.5})$$

Since

$$\left. \begin{aligned} C^t(0) &= 6 \left(P_{k,1}^t - 2P_{k,2}^t + P_{k,3}^t \right) = 6 \overrightarrow{Q_{i,next}^t P_{k,3}^t}, \\ C^b(0) &= 6 \left(P_{k,1}^b - 2P_{k,2}^b + P_{k,3}^b \right) = 6 \overrightarrow{Q_{i,next}^b P_{k,3}^b} \end{aligned} \right\} \quad (\text{C.6})$$

Eq. (C.5) can be reorganized as:

$$\frac{d^2Ori_k(u=0)}{ds^2} = \frac{1}{\|P_{k,3}^t - P_{k,3}^b\|} \left[\frac{\left(6\overrightarrow{Q_{i,next}^t P_{k,3}^t} - 6\overrightarrow{Q_{i,next}^b P_{k,3}^b}\right)}{\left\|3\overrightarrow{P_{k,3}^b P_{k,2}^b}\right\|^2} - \left(3\overrightarrow{P_{k,3}^t P_{k,2}^t} - 3\overrightarrow{P_{k,3}^b P_{k,2}^b}\right) \frac{\left\langle 3\overrightarrow{P_{k,3}^b P_{k,2}^b}, 6\overrightarrow{Q_{i,next}^b P_{k,3}^b} \right\rangle}{\left\|3\overrightarrow{P_{k,3}^b P_{k,2}^b}\right\|^4} \right] \quad (C.7)$$

Similarly, d^2Ori/ds of the transition Bezier curve $B_{k-1}^b(u)$ at its end point ($u = 1$) is evaluated as:

$$\frac{d^2Ori_{k-1}(u=1)}{ds^2} = \frac{1}{\left\| P_{k-1,3}^t - P_{k-1,3}^b \right\|} \left[\frac{\left(6Q_{i,pre}^t P_{k-1,3}^t - 6Q_{i,pre}^b P_{k-1,3}^b \right)}{\left\| 3P_{k-1,2}^b P_{k-1,3}^b \right\|^2} - \left(3P_{k-1,2}^t P_{k-1,3}^t - 3P_{k-1,2}^b P_{k-1,3}^b \right) \frac{\left\langle 3P_{k-1,2}^b P_{k-1,3}^b, 6Q_{i,pre}^b P_{k-1,3}^b \right\rangle}{\left\| 3P_{k-1,2}^b P_{k-1,3}^b \right\|^4} \right] \quad (C.8)$$

The $d^2\text{Ori}/ds^2$ must match at the connection point $P_{k,3}^b$ (i.e. $d^2\text{Ori}_k(u=0)/ds^2 = d^2\text{Ori}_{k-1}(u=1)/ds^2$). Combining $P_{k,2}^t - P_{k,3}^t = P_{k-1,3}^t - P_{k-1,2}^t$,

$$\left. \begin{aligned} \overrightarrow{Q_{i,pre}^t P_{k-1,3}^t} &= \overrightarrow{Q_{i,next}^t P_{k,3}^t}, \\ \overrightarrow{Q_{i,pre}^b P_{k-1,3}^b} &= \overrightarrow{Q_{i,next}^b P_{k,3}^b} \end{aligned} \right\} \quad (C.9)$$

which leads to

$$\left. \begin{aligned} Q_{i,pre}^t &= Q_{i,next}^t = Q_i^t \\ Q_{i,pre}^b &= Q_{i,next}^b = Q_i^b \end{aligned} \right\} \quad (\text{C.10})$$

Hence, $\alpha = 1$.

Appendix D

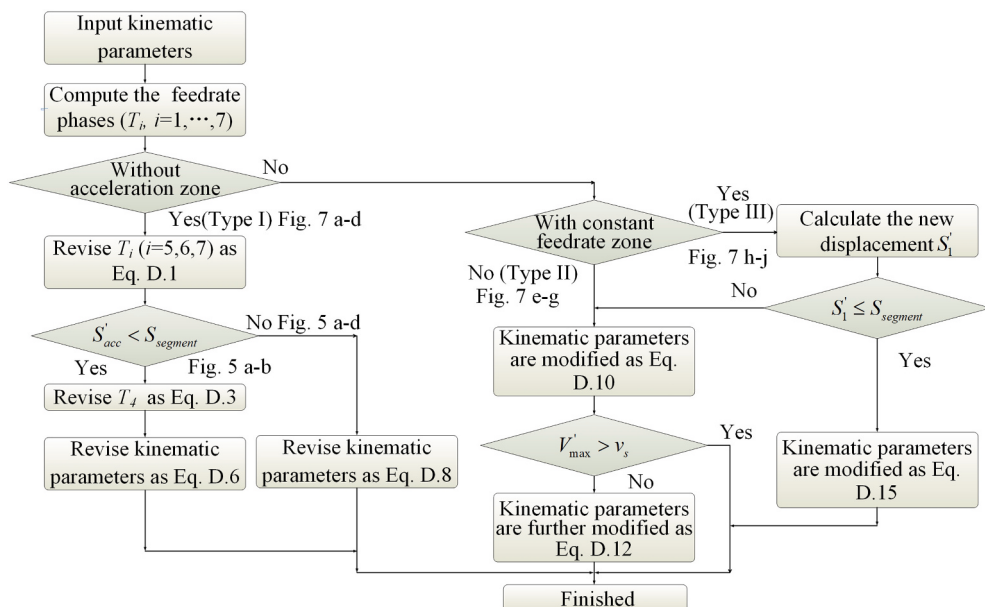


Fig. D.1. Flowchart of jerk-limited feedrate planning algorithm with feedrate phases adjustment ($v_s > v_e$).

In Fig. 7, the start feedrate is higher than the end feedrate (i.e. $v_s > v_e$). Fig. 7(a–d), (e–g) and (h–j) are the feedrate profiles without the acceleration zone (feedrate type I), feedrate profiles with an acceleration zone and a deceleration zone (feedrate type II) and feedrate profiles that contain an

acceleration zone, a constant-speed zone and a deceleration zone (feedrate type III) respectively. Similar to the case where the start feedrate is lower than the end feedrate in previous Section 3.1, the flowchart of the proposed jerk-limited feedrate planning algorithm for $v_s > v_e$ is summarized in Fig. D.1 with the following highlights:

- (1) The kinematic parameters of the current feedrate planning unit, including the start feedrate (v_s), end feedrate (v_e), feedrate, acceleration and jerk limits (F_c, A_{\max}, J_{\max}), and toolpath length of the feedrate planning unit (S_{segment}), are first set. Then the jerk-limited feedrate planning algorithm is implemented on the unit, i.e. $T_i (i = 1, \dots, 7)$ are calculated (Table D.1).

Table D.1

Non-zero feedrate phases for different feedrate profile types ($v_s > v_e$).

Type I	$\text{if } v_s - v_e > A_{\max}^2/J_{\max}, T_5 = T_7 = A_{\max}/J_{\max}, T_6 = (v_s - v_e)/A_{\max} - T_5, \text{else } T_5 = T_7 = \sqrt{(v_s - v_e)/J_{\max}}.$ $\text{if } S_{\text{dec}} = S_{\text{segment}}, T_4 = 0, \text{else } T_4 = (S_{\text{segment}} - S_{\text{dec}})/v_s.$
Type II	$\text{if } V_{\max} - v_s > A_{\max}^2/J_{\max}, T_1 = T_3 = A_{\max}/J_{\max}, T_2 = (V_{\max} - v_s)/A_{\max} - T_1, \text{else } T_1 = T_3 = \sqrt{(V_{\max} - v_s)/J_{\max}}.$ $\text{if } V_{\max} - v_e > A_{\max}^2/J_{\max}, T_5 = T_7 = A_{\max}/J_{\max}, T_6 = (V_{\max} - v_e)/A_{\max} - T_5, \text{else } T_5 = T_7 = \sqrt{(V_{\max} - v_e)/J_{\max}}.$
Type III	$\text{if } V_{\max} - v_s > A_{\max}^2/J_{\max}, T_1 = T_3 = A_{\max}/J_{\max}, T_2 = (V_{\max} - v_s)/A_{\max} - T_1, \text{else } T_1 = T_3 = \sqrt{(V_{\max} - v_s)/J_{\max}}.$ $\text{if } V_{\max} - v_e > A_{\max}^2/J_{\max}, T_5 = T_7 = A_{\max}/J_{\max}, T_6 = (V_{\max} - v_e)/A_{\max} - T_5, \text{else } T_5 = T_7 = \sqrt{(V_{\max} - v_e)/J_{\max}}.$ $T_4 = (S_{\text{segment}} - S_{\text{acc}} - S_{\text{dec}})/V_{\max}.$

- (2) In Fig. 7(a–d), the initial scheduled feedrate profiles only have deceleration and constant feedrate zones, i.e. $T_i = 0 (i = 1, \dots, 3)$. Therefore, only $T_i (i = 4, 5, 6, 7)$ needs to be adjusted to have integer multiples of the interpolation period, where $T_i (i = 5, 6, 7)$ is first revised as:

$$T'_i = \text{ceil}(T_i/T)T \quad (\text{D.1})$$

Combing Eq. (19), the corresponding tool travel displacement in the revised feedrate phases $T'_i (i = 5, 6, 7)$ is calculated as:

$$S'_{\text{dec}} = \frac{v_e + V_{\max}}{2} (2T'_5 + T'_6) \quad (\text{D.2})$$

which should be no longer than the toolpath length of the current feedrate planning unit (S_{segment}) and determines the value of the revised feedrate phase T_4 . Hence,

Case $S'_{\text{dec}} < S_{\text{segment}}$ holds (Fig. 7a–b): The adjusted feedrate profile must have a constant feedrate zone, and the revised T_4 (T'_4) is evaluated as:

$$T'_4 = \left(\frac{S_{\text{segment}} - S'_{\text{dec}}}{V_{\max}T} \right) T = \left(\frac{S_{\text{segment}} - b'}{V_{\max}T} - \frac{a'}{T} \right) T \quad (\text{D.3})$$

where $a' = (T'_5 + T'_6/2)$, $b' = v_e(T'_5 + T'_6/2)$.

Since the toolpath length of each feedrate planning unit (S_{segment}) is constant and only determined by the smoothed toolpath, the maximum velocity (V_{\max}) on the current feedrate planning unit needs further adjustment for the revised $T'_i (i = 4, 5, 6, 7)$ to ensure tool travel displacement shorter than or equal to S_{segment} . Considering,

$$\left. \begin{aligned} S'_{\text{dec}} &= \frac{v'_e + V'_{\max}}{2} (2T'_5 + T'_6) \\ S_{\text{segment}} &= S'_{\text{dec}} + V'_{\max} T'_4 \end{aligned} \right\} \quad (\text{D.4})$$

The V_{\max} is revised as:

$$V'_{\max} = \frac{S_{\text{segment}} - S'_{\text{dec}}}{T'_4} = \frac{S_{\text{segment}} - v_e(T'_5 + T'_6/2)}{T'_4 + T'_5 + T'_6/2} \quad (\text{D.5})$$

Since the revised feedrate phase $T'_i (i = 4, 5, 6, 7)$ and maximum velocity V'_{\max} are now different than the initial scheduled feedrate phases $T_i (i = 4, 5, 6, 7)$ and V_{\max} , while the toolpath length of the current feedrate planning unit is unchanged, it is necessary to modify the start feedrate (v_s), acceleration limit (A_{dec}) and jerk limits (J_5, J_7). Combing with Table 1 and Eq. (D.4), the modified end feedrate (v'_s), acceleration limit (A'_{dec}) and jerk limits (J'_5, J'_7) are evaluated as:

$$\left. \begin{aligned} v'_s &= V'_{\max} = \frac{S_{\text{segment}} - v_e(T'_5 + T'_6/2)}{T'_4 + T'_5 + T'_6/2} \\ A'_{\text{dec}} &= \frac{v'_e - V'_{\max}}{T'_5 + T'_6} \\ J'_5 &= -J'_7 = \frac{A'_{\text{dec}}}{T'_5} \end{aligned} \right\} \quad (\text{D.6})$$

Case $S'_{\text{acc}} \geq S_{\text{segment}}$ holds (Fig. 7a–d): The adjusted feedrate profile does not have the constant feedrate zone, and the initial scheduled T_4 is revised as $T'_4 = 0$. To ensure the S'_{dec} (Eq. D.4) no longer than S_{segment} , the maximum velocity (V'_{\max}) on the current feedrate planning unit needs further adjustment for the revised $T'_i(5, 6, 7)$. Considering Eq. (20), the V'_{\max} is revised as:

$$V'_{\max} = \frac{S_{\text{segment}} - b'}{a'} \quad (\text{D.7})$$

where $a' = (T'_5 + T'_6/2)$, $b' = v_e(T'_5 + T'_6/2)$.

Combing Table 1 and Eq. (D.2) where S'_{dec} is set to be equal to S_{segment} , the modified end feedrate (v'_s), acceleration limit (A'_{dec}) and jerk limits (J'_5, J'_7) for revised feedrate phases $T'_i(5, 6, 7)$ are evaluated as:

$$\left. \begin{aligned} v'_s &= V'_{\max} = \frac{S_{\text{segment}} - b'}{a'} \\ A'_{\text{dec}} &= \frac{v'_e - V'_{\max}}{T'_5 + T'_6}, \quad J'_5 = -J'_7 = A'_{\text{dec}} / T'_5 \end{aligned} \right\} \quad (\text{D.8})$$

where $a' = (T'_5 + T'_6/2)$, $b' = v_e(T'_5 + T'_6/2)$.

Hence, the revised feedrate phases and kinematic parameters are summarized as:

$$\left. \begin{aligned} S'_{\text{dec}} < S_{\text{segment}} & \left\{ \begin{aligned} T'_i &= \text{ceil}(T_i/T)T \quad (i = 5, 6, 7), T'_4 = \left(\frac{S_{\text{segment}} - b'}{V'_{\max} T} - \frac{a'}{T} \right) T \\ T'_1 &= T'_2 = T'_3 = 0, \\ v'_s &= V'_{\max} = \frac{S_{\text{segment}} - v_e(T'_5 + T'_6/2)}{T'_4 + T'_5 + T'_6/2}, A'_{\text{dec}} = \frac{v'_e - V'_{\max}}{T'_5 + T'_6}, J'_5 = -J'_7 = \frac{A'_{\text{dec}}}{T'_5} \end{aligned} \right\} \\ S'_{\text{dec}} \geq S_{\text{segment}} & \left\{ \begin{aligned} T'_i &= \text{ceil}(T_i/T)T \quad (i = 5, 6, 7), T'_1 = T'_2 = T'_3 = T'_4 = 0 \\ v'_s &= V'_{\max} = \frac{S_{\text{segment}} - b'}{a'} \\ A'_{\text{dec}} &= \frac{v'_e - V'_{\max}}{T'_5 + T'_6}, \quad J'_5 = -J'_7 = A'_{\text{dec}} / T'_5 \end{aligned} \right\} \end{aligned} \right\} \quad (\text{D.9})$$

where $a' = (T'_5 + T'_6/2)$, $b' = v_e(T'_5 + T'_6/2)$.

(3) For the feedrate profile without a constant feedrate zone, i.e. only $T_4 = 0$ (Type II, Fig. 7e–g), the initial scheduled feedrate phases T_i ($i = 1, 2, 3, 5, 6, 7$) are revised as $T'_i = \text{ceil}(T_i/T)$ ($i = 1, 2, 3, 5, 6, 7$), and the revised maximum velocity (V'_{\max}), acceleration limits ($A'_{\text{acc}}, A'_{\text{dec}}$) and jerk limits (J'_1, J'_3, J'_5, J'_7) are evaluated as:

$$\left. \begin{aligned} V'_{\max} &= \frac{S_{\text{segment}} - b'}{a'} \\ A'_{\text{acc}} &= \frac{V'_{\max} - v_s}{T'_1 + T'_2}, J'_1 = -J'_3 = \frac{A'_{\text{acc}}}{T'_1} \\ A'_{\text{dec}} &= \frac{v'_e - V'_{\max}}{T'_5 + T'_6}, \quad J'_5 = -J'_7 = A'_{\text{dec}} / T'_5 \end{aligned} \right\} \quad (\text{D.10})$$

where $a' = (T'_1 + T'_5 + T'_2/2 + T'_6/2)$, $b' = v_s(T'_1 + T'_2/2) + v_e(T'_5 + T'_6/2)$.

The revised V'_{\max} must be higher than v_s , otherwise, V'_{\max} should be updated as:

$$V'_{\max} = \frac{S_{\text{segment}} - v_e(T'_5 + T'_6/2)}{T'_5 + T'_6/2 + T'_4} \quad (\text{D.11})$$

where $T'_4 = T'_1 + T'_2 + T'_3$.

Leading to the modified start velocity (v'_s) and further updated acceleration limit (A'_{dec}) and jerk limits (J'_5, J'_7) as:

$$\left. \begin{array}{l} v'_s = V'_{\max} = \frac{S_{\text{segment}} - v_e(T'_5 + T'_6/2)}{T'_5 + T'_6/2 + T'_4} \\ A'_{\text{dec}} = \frac{V'_{\max} - v_e}{T'_5 + T'_6}, J'_5 = -J'_7 = \frac{A'_{\text{dec}}}{T'_5} \end{array} \right\} \quad (\text{D.12})$$

Hence, the complete revision equations for the Type II feedrate profiles are concluded as:

$$\left. \begin{array}{l} \text{when } V'_{\max} > v_s \left\{ \begin{array}{l} T'_1 = \text{ceil}\left(\frac{T'_i}{T}\right)T \quad (i = 1, 2, 3, 5, 6, 7) \quad T'_4 = 0 \\ V'_{\max} = \frac{S_{\text{segment}} - b'}{a'} \\ A'_{\text{acc}} = \frac{V'_{\max} - v_s}{T'_1 + T'_2}, J'_1 = -J'_3 = \frac{A'_{\text{acc}}}{T'_1}, A'_{\text{dec}} = \frac{v'_e - V'_{\max}}{T'_5 + T'_6}, J'_5 = -J'_7 = \frac{A'_{\text{dec}}}{T'_5} \end{array} \right\} \\ \text{when } V'_{\max} \leq v_s \left\{ \begin{array}{l} T'_1 = \text{ceil}\left(\frac{T'_i}{T}\right)T \quad (i = 5, 6, 7) \\ T'_4 = T'_1 + T'_2 + T'_3, \quad T'_1 = T'_2 = T'_3 = 0, \\ V'_{\max} = \frac{S_{\text{segment}} - v_e(T'_5 + T'_6/2)}{T'_5 + T'_6/2 + T'_4}, v'_s = V'_{\max} \\ A'_{\text{dec}} = \frac{V'_{\max} - v_e}{T'_5 + T'_6}, J'_5 = -J'_7 = \frac{A'_{\text{dec}}}{T'_5} \end{array} \right\} \end{array} \right\} \quad (\text{D.13})$$

where $a' = (T'_1 + T'_5 + T'_2/2 + T'_6/2)$, $b' = v_s(T'_1 + T'_2/2) + v_e(T'_5 + T'_6/2)$.

(4) For the complete feedrate profile, i.e. a feedrate profile with an acceleration zone, a constant feedrate zone and a deceleration zone (Type III, Fig. 7h–j), the tool travel displacement in feedrate phases $T'_i (i = 1, 2, 3, 5, 6, 7)$ (S'_1) is calculated and compared against the toolpath length of the current feedrate planning unit S_{segment} . If $S'_1 \leq S_{\text{segment}}$ holds, the revised feedrate phase T'_4 (T'_4) is evaluated as:

$$T'_4 = \text{ceil}\left(\frac{S_{\text{segment}} - S'_1}{V'_{\max}T}\right)T = \text{ceil}\left(\frac{S_{\text{segment}} - b'}{V'_{\max}T} - \frac{a'}{T}\right)T \quad (\text{D.14})$$

where $a' = (T'_1 + T'_5 + T'_2/2 + T'_6/2)$, $b' = v_s(T'_1 + T'_2/2) + v_e(T'_5 + T'_6/2)$.

Leading to revised maximum velocity (V'_{\max}), acceleration limits ($A'_{\text{acc}}, A'_{\text{dec}}$) and jerk limits (J'_1, J'_3, J'_5, J'_7) which are evaluated as:

$$\left. \begin{array}{l} V'_{\max} = \frac{S_{\text{segment}} - b'}{T'_4 + a'} \\ A'_{\text{acc}} = \frac{V'_{\max} - v_s}{T'_1 + T'_2}, J'_1 = -J'_3 = \frac{A'_{\text{acc}}}{T'_1} \\ A'_{\text{dec}} = \frac{v_e - V'_{\max}}{T'_5 + T'_6}, J'_5 = -J'_7 = \frac{A'_{\text{dec}}}{T'_5} \end{array} \right\} \quad (\text{D.15})$$

where $a' = (T'_1 + T'_5 + T'_2/2 + T'_6/2)$, $b' = v_s(T'_1 + T'_2/2) + v_e(T'_5 + T'_6/2)$.

Otherwise, the maximum velocity must be reduced as Eq. (D.10). Then, the updated feedrate phases and revised kinematic parameters are obtained as Eq. (D.13). In summary, the revised kinematic parameters and feedrate phases for the Type III feedrate profiles are summarized as:

$$\left\{ \begin{array}{l} T'_i = \text{ceil}(T_i/T)T \quad (i = 1, 2, 3, 5, 6, 7), T'_4 = \text{ceil}\left(\frac{S_{\text{segment}} - b'}{V_{\max} T} - \frac{a'}{T}\right)T \\ V'_{\max} = \frac{S_{\text{segment}} - b'}{T'_4 + a'}, \\ A'_{acc} = \frac{V'_{\max} - v_s}{T'_1 + T'_2}, J'_1 = -J'_3 = \frac{A'_{acc}}{T'_1}, A'_{dec} = \frac{v_e - V'_{\max}}{T'_5 + T'_6}, J'_5 = -J'_7 = \frac{A'_{dec}}{T'_5} \end{array} \right\} \quad (\text{D.16})$$

$S'_1 \leq S_{\text{segment}}$

$S'_1 > S_{\text{segment}}$ Eq.(D.13)

where $a' = (T'_1 + T'_5 + T'_2/2 + T'_6/2)$, $b' = v_s(T'_1 + T'_2/2) + v_e(T'_5 + T'_6/2)$.

References

- [1] Erkorkmaz K, Altintas Y. High speed CNC system design. Part I: jerk limited trajectory generation and quintic spline interpolation. Int J Mach Tools Manuf 2001;41(09):1323–45. [https://doi.org/10.1016/S0890-6955\(01\)00002-5](https://doi.org/10.1016/S0890-6955(01)00002-5).
- [2] Yau HT, Wang J. Fast Bezier interpolator with real-time lookahead function for high-accuracy machining. Int J Mach Tools Manu 2007;47(10):1518–29. <https://doi.org/10.1016/j.ijmachtools.2006.11.010>.
- [3] Bi Q, Huang J, Lu Y, Zhu L, Ding H. A general, fast and robust B-spline fitting scheme for micro-line tool path under chord error constraint. Sci China Technol Sci 2019;62:321–32. <https://doi.org/10.1007/s11431-018-9374-6>.
- [4] Du X, Huang J, Zhu L, Ding H. An error-bounded B-spline curve approximation scheme using dominant points for CNC interpolation of micro-line toolpath. Robot Cim Int Manuf 2020;64:101930. <https://doi.org/10.1016/j.rcim.2019.101930>.
- [5] Liu M, Huang Y, Yin L, Guo J, Shao X, Zhang G. Development and implementation of a NURBS interpolator with smooth feedrate scheduling for CNC machine tools. Int J Mach Tools Manuf 2014;87:1–15. <https://doi.org/10.1016/j.ijmachtools.2014.07.002>.
- [6] Ho MC, Hwang YR, Hu CH. Five-axis tool orientation smoothing using quaternion interpolation algorithm. Int J Mach Tools Manuf 2003;43(12):1259–67. [https://doi.org/10.1016/S0890-6955\(03\)00107-X](https://doi.org/10.1016/S0890-6955(03)00107-X).
- [7] Wang H, Jiang X. Geometric error identification of five-axis machine tools using dual quaternion. Int J Mech Sci 2022;229:107522. <https://doi.org/10.1016/j.ijmecsci.2022.107522>.
- [8] Fleisig RV, Spence AD. A constant feed and reduced angular acceleration interpolation algorithm for multi-axis machining. Comput Aided Des 2001;33(01):1–15. [https://doi.org/10.1016/S0010-4485\(00\)00049-X](https://doi.org/10.1016/S0010-4485(00)00049-X).
- [9] Yuen A, Zhang K, Altintas Y. Smooth trajectory generation for five-axis machine tools. Int J Mach Tools Manuf 2013;71:11–9. <https://doi.org/10.1016/j.ijmachtools.2013.04.002>.
- [10] Li D, Zhang W, Zhou W, Shang T, Fleischer J. Dual NURBS path smoothing for 5-axis linear path of flank milling. Int J Precis Eng Manuf 2018;19:1811–20. <https://doi.org/10.1007/s12541-018-0209-6>.
- [11] Langeron JM, Duc E, Lartigue C, Bourdet P. A new format for 5-axis tool path computation, using Bspline curves. Comput Aided Des 2004;36(12):1219–29. <https://doi.org/10.1016/j.cad.2003.12.002>.
- [12] Min K, Lee CH, Yan C, Fan W, Hu P. Six-dimensional B-spline fitting method for five-axis tool paths. Int J Adv Manuf Technol 2020;107:2041–54. <https://doi.org/10.1007/s00170-020-05139-7>.
- [13] Sun S, Altintas Y. A G^3 continuous tool path smoothing method for 5-axis CNC machining. Cirp J Manuf Sci Technol 2021;32:529–49. <https://doi.org/10.1016/j.cirpj.2020.11.002>.
- [14] Tajima S, Sencer B. Online interpolation of 5-axis machining toolpaths with global blending. Int J Mach Tools Manuf 2022;175:103862. <https://doi.org/10.1016/j.ijmachtools.2022.103862>.
- [15] Fan W, Lee CH, Chen JH. A realtime curvature-smooth interpolation scheme and motion planning for CNC machining of short line segments. Int J Mach Tools Manuf 2015;96:27–46. <https://doi.org/10.1016/j.ijmachtools.2015.04.009>.
- [16] Sun S, Lin H, Zheng L, Yu J, Hu Y. A real-time and look-ahead interpolation methodology with dynamic B-spline transition scheme for CNC machining of short line segments. Int J Adv Manuf Technol 2016;84:1359–70. <https://doi.org/10.1007/s00170-015-7776-9>.
- [17] Zhang Y, Zhao M, Ye P, Zhang H. A G^4 continuous B-spline transition algorithm for CNC machining with jerk-smooth feedrate scheduling along linear segments. Comput Aided Des 2019;115:231–43. <https://doi.org/10.1016/j.cad.2019.04.004>.
- [18] Huang N, Hua L, Huang X, Zhang Y, Zhu L, Biermann D. B-spline-based corner smoothing method to decrease the maximum curvature of the transition curve. J Manuf Sci Eng 2022;144(05):054503. <https://doi.org/10.1115/1.4052708>.
- [19] Du X, Wang B. A C^3 -continuous NURBS transition scheme for the CNC machining of short linear segments. Precis Eng 2022;73:1–10. <https://doi.org/10.1016/j.precisioneng.2021.08.016>.
- [20] Beudaert X, Laverne S, Tournier C. 5-axis local corner rounding of linear tool path discontinuities. Int J Mach Tools Manuf 2013;73:9–16. <https://doi.org/10.1016/j.ijmachtools.2013.05.008>.
- [21] Bi Q, Shi J, Wang Y, Zhu L, Ding H. Analytical curvature-continuous dual-Bézier corner transition for five-axis linear tool path. Int J Mach Tools Manuf 2015;91:96–108. <https://doi.org/10.1016/j.ijmachtools.2015.02.002>.
- [22] Tulsyan S, Altintas Y. Local toolpath smoothing for five-axis machine tools. Int J Mach Tools Manuf 2015;96:15–26. <https://doi.org/10.1016/j.ijmachtools.2015.04.014>.
- [23] Yang J, Yuen A. An analytical local corner smoothing algorithm for five-axis CNC machining. Int J Mach Tools Manuf 2017;123:22–35. <https://doi.org/10.1016/j.ijmachtools.2017.07.007>.
- [24] Sun S. A G^3 continuous five-axis tool path corner smoothing method with improved machining efficiency and accurately controlled deviation of tool axis orientation. Int J Adv Manuf Technol 2022;119:7003–24. <https://doi.org/10.1007/s00170-021-08227-4>.
- [25] Yang K, Sukkarieh S. An analytical continuous-curvature path-smoothing algorithm. IEEE Trans Robot 2010;26(3):561–8. <https://doi.org/10.1109/TRO.2010.2042990>.
- [26] Chen T, Cai Y, Chen L, Xu X. Trajectory and velocity planning method of emergency rescue vehicle based on segmented three-dimensional quartic Bezier curve. IEEE Trans Intell Transp 2023;24(3):3461–75. <https://doi.org/10.1109/TITS.2022.3224785>.
- [27] Yang J, Li D, Ye C, Ding H. An analytical C^3 continuous tool path corner smoothing algorithm for 6R robot manipulator. Robot Cim Int Manuf 2020;64:101947. <https://doi.org/10.1016/j.rcim.2020.101947>.
- [28] Xie Z, Xie F, Liu X, Wang J. Global G^3 continuity toolpath smoothing for a 5-DoF machining robot with parallel kinematics. Robot Cim-Int Manuf 2021;67:102018. <https://doi.org/10.1016/j.rcim.2020.102018>.
- [29] Liu H, Li G, Xiao J. A C^3 continuous toolpath corner smoothing method for a hybrid machining robot. J Manuf Process 2022;75:1072–88. <https://doi.org/10.1016/j.jmapro.2021.12.057>.
- [30] Souza AF, Coelho RT. Experimental investigation of feed rate limitations on high speed milling aimed at industrial applications. Int J Adv Manuf Technol 2007;32:1104–14. <https://doi.org/10.1007/s00170-006-0445-2>.
- [31] Dong J, Wang T, Li B, Ding Y. Smooth feedrate planning for continuous short line tool path with contour error constraint. Int J Mach Tools Manuf 2014;76:1–12. <https://doi.org/10.1016/j.ijmachtools.2013.09.009>.
- [32] Han GC, Kim DII, Kim HG, Nam K, Choi BK, Kim SK. A high speed machining algorithm for CNC machine tools. In: Conference proceedings of the 25th annual conference of the IEEE Industrial Electronics Society; 1999 Nov 29–Dec 03; San Jose, CA, USA. New York: IEEE; 1999. <https://doi.org/10.1109/IECON.1999.819445>.
- [33] Luo F, Zhou Y, Yin J. A universal velocity profile generation approach for high-speed machining of small line segments with look-ahead. Int J Adv Manuf Technol 2007;35:505–18. <https://doi.org/10.1007/s00170-006-0735-8>.
- [34] Zhong W, Luo X, Chang W, Ding F, Cai Y. A real-time interpolator for parametric curves. Int J Mach Tools Manuf 2018;125:133–45. <https://doi.org/10.1016/j.ijmachtools.2017.11.010>.
- [35] Yan G, Zhang Y, Li C, Xu J. Asymmetrical transition-based corner rounding method driven by overlap elimination for CNC machining of short-segmented tool path. J Manuf Process 2022;76:624–37. <https://doi.org/10.1016/j.jmapro.2022.02.022>.
- [36] Yan G, Liang J, Xu J. Overlap classification-based and kinematically coordinated corner rounding using double asymmetrical transitions for five-axis short-segmented tool path. J Manuf Process 2023;85:1077–95. <https://doi.org/10.1016/j.jmapro.2022.12.018>.
- [37] Nam SH, Yang MY. A study on a generalized parametric interpolator with real-time jerk-limited acceleration. Comput Aided Des 2004;36(01):27–36. [https://doi.org/10.1016/S0010-4485\(03\)00066-6](https://doi.org/10.1016/S0010-4485(03)00066-6).

- [38] Lu TC, Chen SL, Yang ECY. Near time-optimal S-curve velocity planning for multiple line segments under axis constraints. *IEEE Trans Ind Electron* 2018;65(12):9582–92. <https://doi.org/10.1109/TIE.2018.2818669>.
- [39] Endo M, Sencer B. Accurate prediction of machining cycle times by data-driven modelling of NC system's interpolation dynamics. *CIRP Ann-Manuf Technol* 2022;71(01):405–8. <https://doi.org/10.1016/j.cirp.2022.04.017>.
- [40] Fan W, Gao X, Yan W, Yuan C. Interpolation of parametric CNC machining path under confined jounce. *Int J Adv Manuf Technol* 2012;62:719–39. <https://doi.org/10.1007/s00170-011-3842-0>.
- [41] Altintas Y, Erkorkmaz K. Feedrate optimization for spline interpolation in high speed machine tools. *CIRP Ann-Manuf Technol* 2003;52(01):297–302. [https://doi.org/10.1016/S0007-8506\(07\)60588-5](https://doi.org/10.1016/S0007-8506(07)60588-5).
- [42] Yeh SS, Hsu PL. The speed-controlled interpolator for machining parametric curves. *Comput Aided Des* 1999;31(05):349–57. [https://doi.org/10.1016/S0010-4485\(99\)00035-4](https://doi.org/10.1016/S0010-4485(99)00035-4).
- [43] Jia Z, Song D, Ma J, Hu G, Su W. A NURBS interpolator with constant speed at feedrate-sensitive regions under drive and contour-error constraints. *Int J Mach Tools Manuf* 2017;116:1–17. <https://doi.org/10.1016/j.ijmachtools.2016.12.007>.
- [44] Zhang G, Gao J, Zhang L, Wang X, Luo Y, Chen X. Generalised NURBS interpolator with nonlinear feedrate scheduling and interpolation error compensation. *Int J Mach Tools Manuf* 2022;183:103956. <https://doi.org/10.1016/j.ijmachtools.2022.103956>.
- [45] Heng M, Erkorkmaz K. Design of a NURBS interpolator with minimal feed fluctuation and continuous feed modulation capability. *Int J Mach Tools Manuf* 2010;50(03):281–93. <https://doi.org/10.1016/j.ijmachtools.2009.11.005>.
- [46] Zhao H, Zhu L, Ding H. A parametric interpolator with minimal feed fluctuation for CNC machine tools using arc-length compensation and feedback correction. *Int J Mach Tools Manuf* 2013;75:1–8. <https://doi.org/10.1016/j.ijmachtools.2013.08.002>.
- [47] Du X, Huang J, Zhu L. A complete S-shape feedrate scheduling approach for NURBS interpolator. *Int J Mach Tools Manuf* 2015;2:206–17. <https://doi.org/10.1016/j.jcde.2015.06.004>.
- [48] Piegl L, Tiller W. The NURBS books. 2nd ed. Berlin: Springer; 1997. <https://doi.org/10.1007/978-3-642-59223-2>.